Molecular Cell, Volume *64*

Supplemental Information

Impact of MicroRNA Levels, Target-Site Complementarity, and Cooperativity on Competing Endogenous RNA-Regulated Gene Expression

Rémy Denzler, Sean E. McGeary, Alexandra C. Title, Vikram Agarwal, David P. Bartel, and Markus Stoffel

Figure S1
Denzler et al.

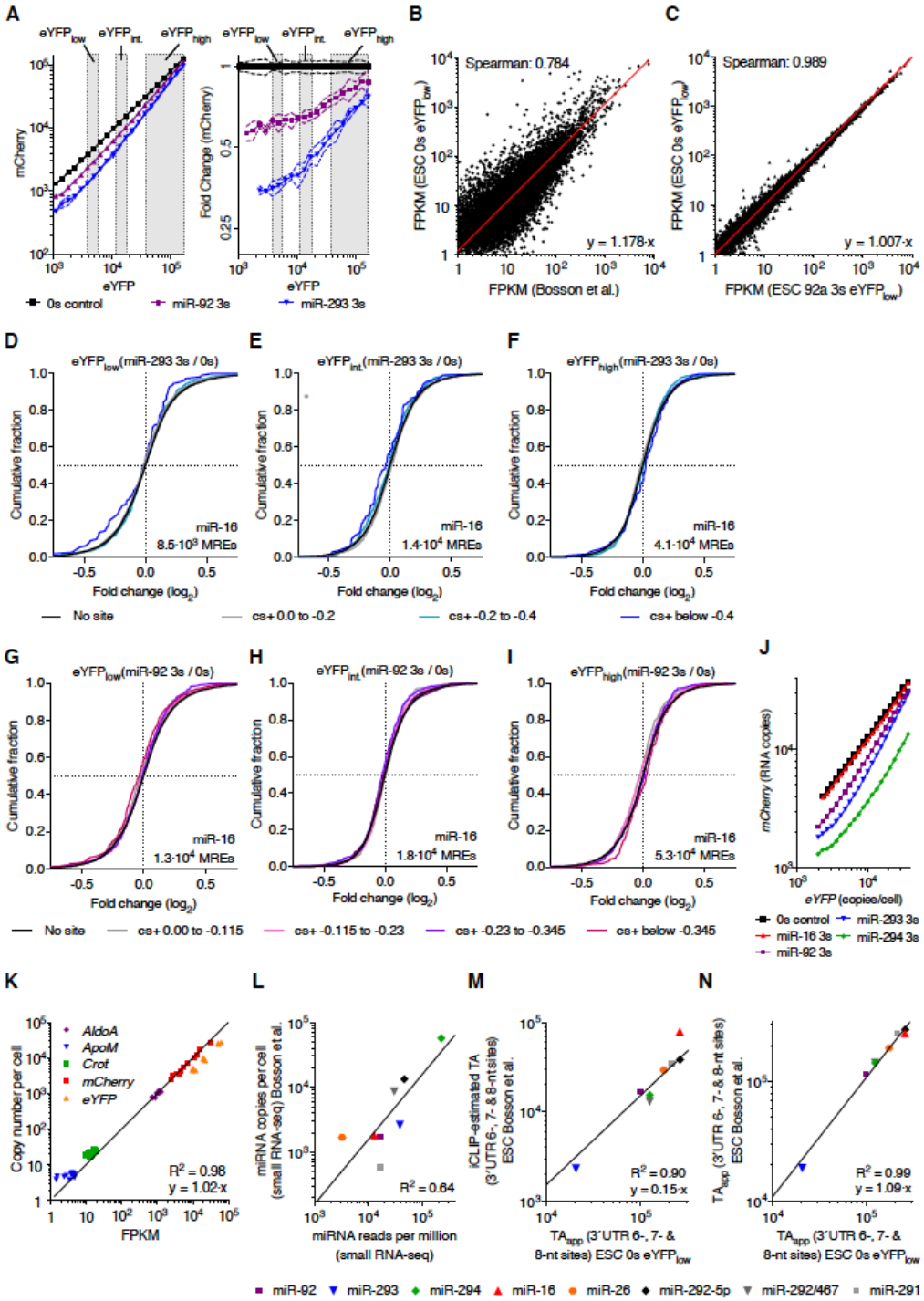

Figure S1. Embryonic Stem Cells (ESCs) Characterized in Bosson et al. (2014) Are Very Similar to ESCs Used in this Study. Related to Figure 1.

(A) ESCs transfected (n = 2) with a 3s reporter for miR-293 (blue) or miR-92 (purple), or a 0s reporter control. Mean mCherry fluorescence (left), and mCherry fluorescence normalized to 0s control (right) across 20 bins of eYFP. In the right panel only fold-change values with mean mCherry expression above 0.8×10^3 are shown. Cells were analyzed and sorted into three bins based on their eYFP expression. The respective gates for $eYFP_{low}$, $eYFP_{int.}$, and $eYFP_{high}$ are highlighted in grey.

(B) Relationship between fragments per kilobase of transcript per million fragments mapped (FPKM) from ESCs of published RNA sequencing (RNA-seq) data (Bosson et al., 2014) and ESCs transfected with the 0s reporter and sorted for low eYFP expressing cells. Line represents linear regression of data points; respective equation is shown.

(C) Relationship between FPKM from RNA-seq data of 0s- and miR-92 3s-transfected ESCs, sorted for low eYFP expressing cells. Line represents linear regression of data points; respective equation is shown.

(D–I) RNA-seq results of sorted ESCs shown in (A) and Figures 1D–1I. ESCs were transfected with a 3s reporter for miR-293 (D–F), or miR-92 (G–I), and gated for cells with low eYFP (D, G), intermediate eYFP (E, H), or high eYFP (F, I) expression. Cumulative distribution function (CDF) of mRNA changes for predicted target genes of miR-16 (D–I) with the indicated context+ score (cs+) bins (color) or for genes with no respective miRNA site (black). miRNA response elements (MREs) per cell evaluated by absolute quantification of *mCherry* by qPCR are shown on each graph. *p < 0.05, **p < 0.01, ***p < 0.001, ****p < 0.0001, one-sided Kolmogorov–Smirnov (K–S) test.

(J) ESCs transfected with the 0s control or 3s reporter constructs (n = 3) with miRNA-binding sites for miR-16, miR-294, miR-293, or miR-92. Protein fluorescence values shown in Figure 1B have been transformed to RNA copies per cell using the equations shown in Figure 1J.

(K) Relationship between FPKM from RNA-seq data and absolute quantification using qPCR. Represented are five genes quantified in 12 ESC samples. Line represents linear regression of data points; respective equation is shown.

(L) Relationship between small RNA-seq data from published ESCs (Bosson et al., 2014) and of ESCs used in this study. See also Table S2.

(M) Relationship between apparent target abundance (TA_{app}) of ESCs transfected with the 0s reporter and sorted for low eYFP expressing cells (ESC 0s $eYFP_{low}$) and iCLIP-estimated TA from published ESCs (Bosson et al., 2014). Line represents linear regression of data points; respective equation is shown.
(N) Relationship between TA_{app} from ESCs of published RNA-seq data (Bosson et al., 2014) and ESC 0s $eYFP_{low}$. FPKM from Bosson et al. (2014) have been transformed using equation shown in Figure (B). Line represents linear regression of data points; respective equation is shown.
Data represent mean ± SEM for Figures (A) and (J).

Figure S2
Denzler et al.

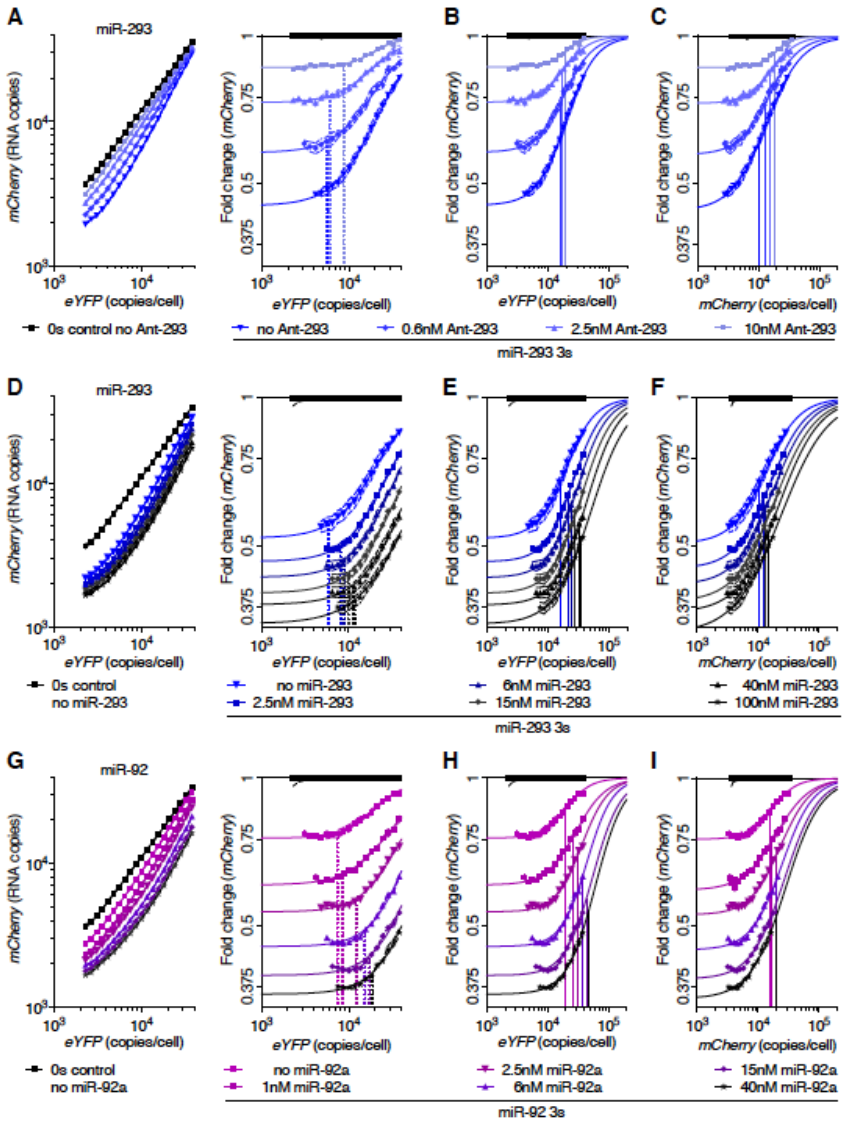

Figure S2. Derepression Threshold Values are Insensitive to Changes in miRNA Activity. Related to Figure 2.

(A–I) ESCs co-transfected with 3s-reporter for miR-293 (A–F), miR-92 (G–I) or respective 0s reporter control, and different concentrations of Antagomir-293 (Ant-293) (n = 3) (A–C), miR-293 (n = 6) (D–F), or miR-92 (n = 6) (G–I). Protein fluorescence values shown in Figures 2A, 2C, and 2E have been transformed to RNA copies per cell using the equations in Figure 1J.

(A, D, G) Mean transformed *mCherry* (left), and *mCherry* normalized to 0s control (right) across 20 bins of *eYFP*. All 3s reporter co-transfections have been normalized to the 0s control with the same respective Ant-293 or miRNA concentration. One representative 0s control where no Ant-293 or miRNA has been transfected is shown. Vertical, dotted lines denote *eYFP* values at the derepression threshold (DRT).

(B, E, H) Data shown in (A, D, G), with vertical lines denoting *eYFP* values where half-maximal derepression (termed half maximal inhibitory concentration, or IC_{50}) is observed. At first glance, a uniform IC_{50} in the context of declining miR-293 activity supports the mixed-affinity model, in which the effective target concentration does not change as miRNA concentrations decreases. However, we cannot exclude the possibility that this interpretation is confounded by the use of co-transfection in this experiment, in which cells that received more plasmid, and thus had more eYFP expression, might have also taken up more Ant-293, and thus would have experienced more miR-293 repression.

(C, F, I) Data shown in Figures 2B, 2D, and 2F, with vertical lines denoting *mCherry* values where half-maximal derepression is observed. Although the IC_{50} values increased only slightly as more miRNA was transfected, interpretation was again potentially confounded by co-transfection of plasmid and miRNA, in which cells that received more plasmid might have also received more miRNA.

Data represent mean ± SEM for all panels.

Figure S3
Denzler et al.

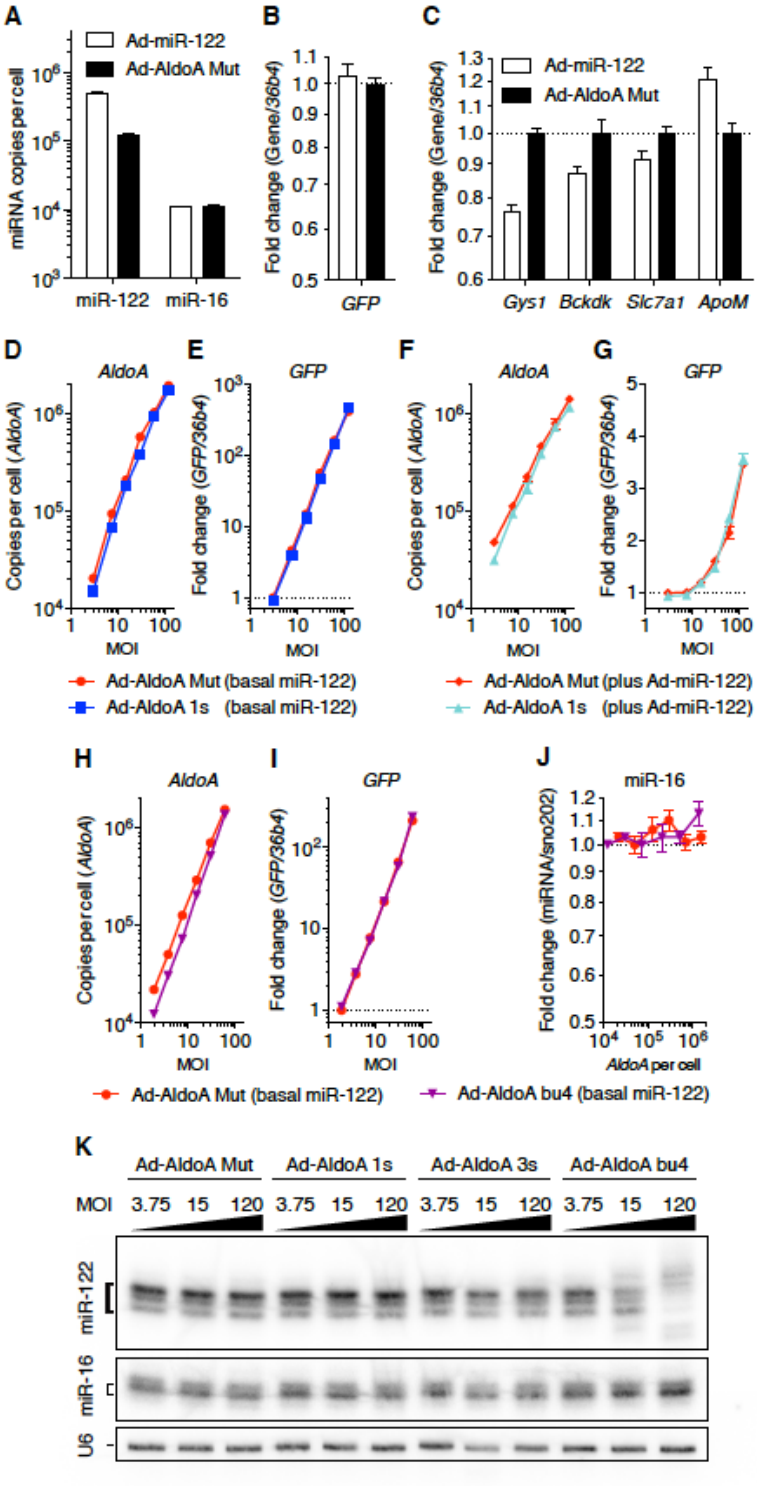

Figure S3. Increasing miR-122 Levels Increases miR-122 Target Gene Repression. Related to Figure 3.

(A–C) Primary hepatocytes (n = 4) infected at a multiplicity of infection (MOI) of 50 with an adenovirus expressing miR-122 (Ad-miR-122) or with Ad-AldoA Mut. Absolute miRNA copy numbers per cell (A), relative *GFP* expression (B), or relative expression of miR-122 target genes and control non-target genes (*ApoM*) (C) normalized to Ad-AldoA Mut.

(D–G) Primary hepatocytes (n = 4) infected with different MOIs of Ad-AldoA Mut or 1s at basal miR-122 levels (D, E), or in addition to MOI 50 of Ad-miR-122 (F, G). Absolute copy numbers per cell of *AldoA* (D, F), and relative gene expression of *GFP* (E, G).

(H–J) Primary hepatocytes (n = 4) infected with different MOIs of Ad-AldoA Mut or bu4 at basal miR-122 levels. Absolute copy numbers per cell of *AldoA* (H), relative gene expression of *GFP* (I), and relative expression of miR-16 (J). miRNA expression is relative to the lowest MOI of Ad-AldoA Mut.

(K) Northern blot analysis of miR-122, miR-16 and U6 of hepatocytes infected with MOI 3.75, MOI 15, and MOI 120 of Ad-AldoA Mut, bu4, 1s, or 3s.

GFP expression is relative to Ad-AldoA Mut at the lowest MOI. Data represent mean ± SEM for all panels.

Figure S4
Denzler et al.

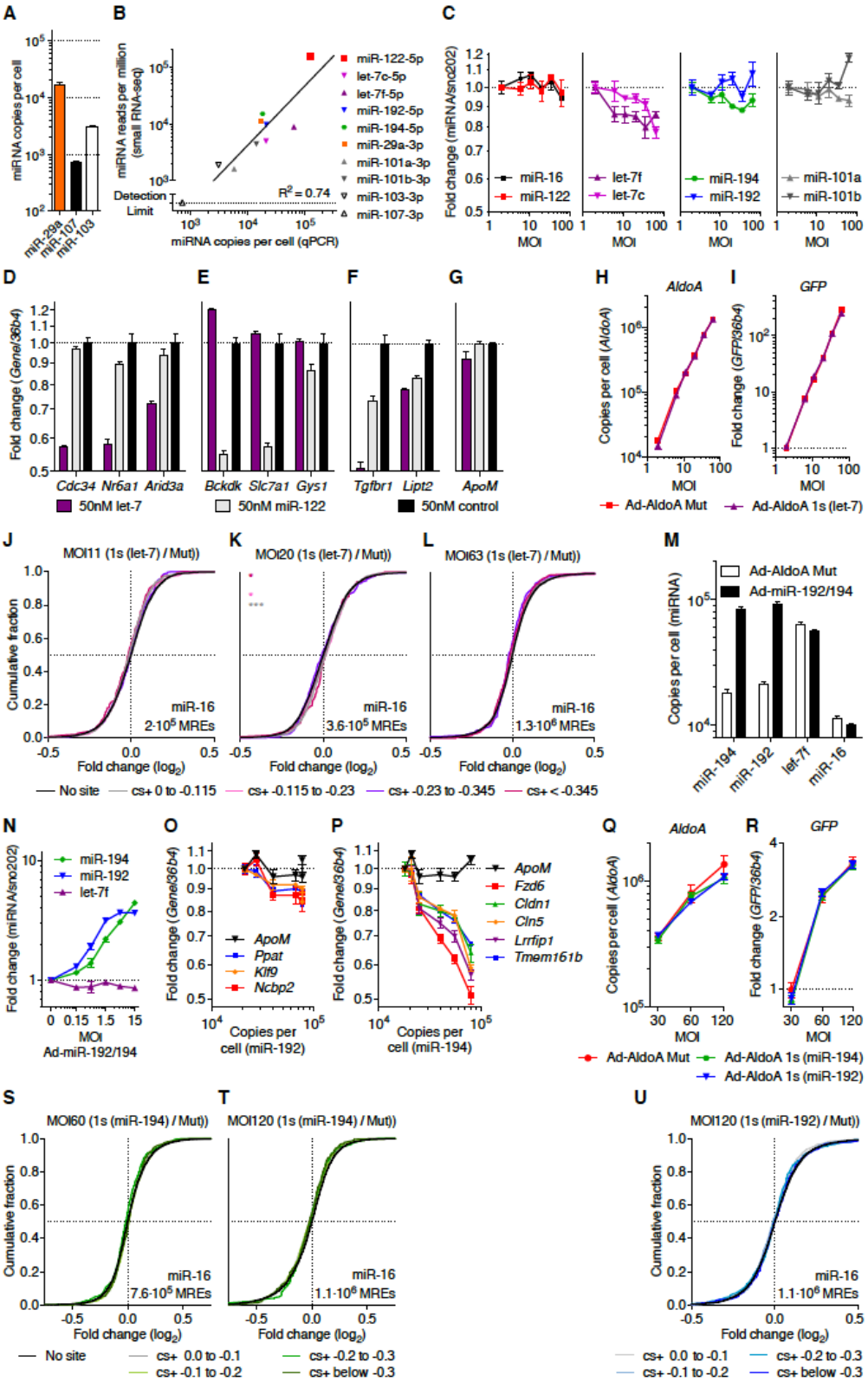

Figure S4. Experimental Evaluation of Predicted Target Genes of miR-122, let-7 miR-192 and miR-194 in Primary Hepatocytes. Related to Figure 4.

(A) Absolute copies per cell of hepatocyte miRNAs (n = 3).

(B) Relationship between miRNA counts from small RNA-seq data and absolute miRNA copies of primary hepatocytes. Line represents linear regression of data points. See also Table S2.

(C) Relative miRNA expression of hepatocytes (n = 4) infected with different MOIs of Ad-AldoA Mut. miRNA expression is relative to Ad-AldoA Mut at MOI 2.

(D–G) Primary hepatocytes transfected with 50 nM of let-7, miR-122, or control siRNA. Relative gene expression of predicted target genes of let-7 (D), of miR-122 (E), or of miR-122 and let-7 (F), and a control non-target gene (*ApoM*) (G). Gene expression is normalized to the negative control.

(H–L) Primary hepatocytes infected with different MOIs of Ad-AldoA Mut or 1s (let-7). Absolute copy numbers per cell of *AldoA* (H), or relative gene expression of *GFP* (I). RNA-seq results (n = 2) from hepatocytes infected with MOI 11 (J), MOI 20 (K), or MOI 63 (L) of Ad-AldoA Mut or 1s (let-7) shown in Figures 4C–4F. CDF of mRNA changes for predicted target genes of miR-16 with the indicated cs+ bins (color) or for genes with no respective miRNA site (black).

(M–P) Primary hepatocytes infected with different MOIs of an adenovirus (n = 4) expressing the bicistronic miR-192/-194 (Ad-miR-192/194) (Krutzfeldt et al., 2012). To control for virus dependent effects, Ad-miR-192/194 was complemented with Ad-AldoA Mut to retrieve a constant MOI of 100. (M) Absolute miRNA copy numbers per cell at MOI 15 of Ad-miR-192/194. Relative miRNA levels (N), relative expression of predicted target genes of miR-192 (O), or of miR-194 (P) and a control non-target gene (*ApoM*) normalized to MOI 100 of Ad-AldoA Mut.

(Q–U) Primary hepatocytes (n = 4) infected with different MOIs of Ad-AldoA Mut, 1s (miR-192), or 1s (miR-194) in addition to MOI 15 Ad-miR-192/194. Absolute copy numbers per cell of *AldoA* (Q), and relative gene expression of *GFP* (R). RNA-seq results (n = 2) from hepatocytes infected with MOI 60 (S) or MOI 120 (T) of Ad-AldoA 1s (miR-194), MOI 120 of Ad-AldoA 1s (miR-192) (U), or respective Ad-AldoA Mut controls. CDF of mRNA changes for predicted target genes of miR-16 with the indicated cs+ bins (color) or for genes with no respective miRNA site (black). *GFP* expression is relative to Ad-AldoA Mut at the lowest MOI. Data represent mean ± SEM for Figures (A), (C–I), and (M–R). MREs per cell evaluated by absolute quantification of *AldoA* by qPCR are shown on each CDF graph. *p < 0.05, **p < 0.01, ***p < 0.001, ****p < 0.0001, one-sided K–S test.

Figure S5
Denzler et al.

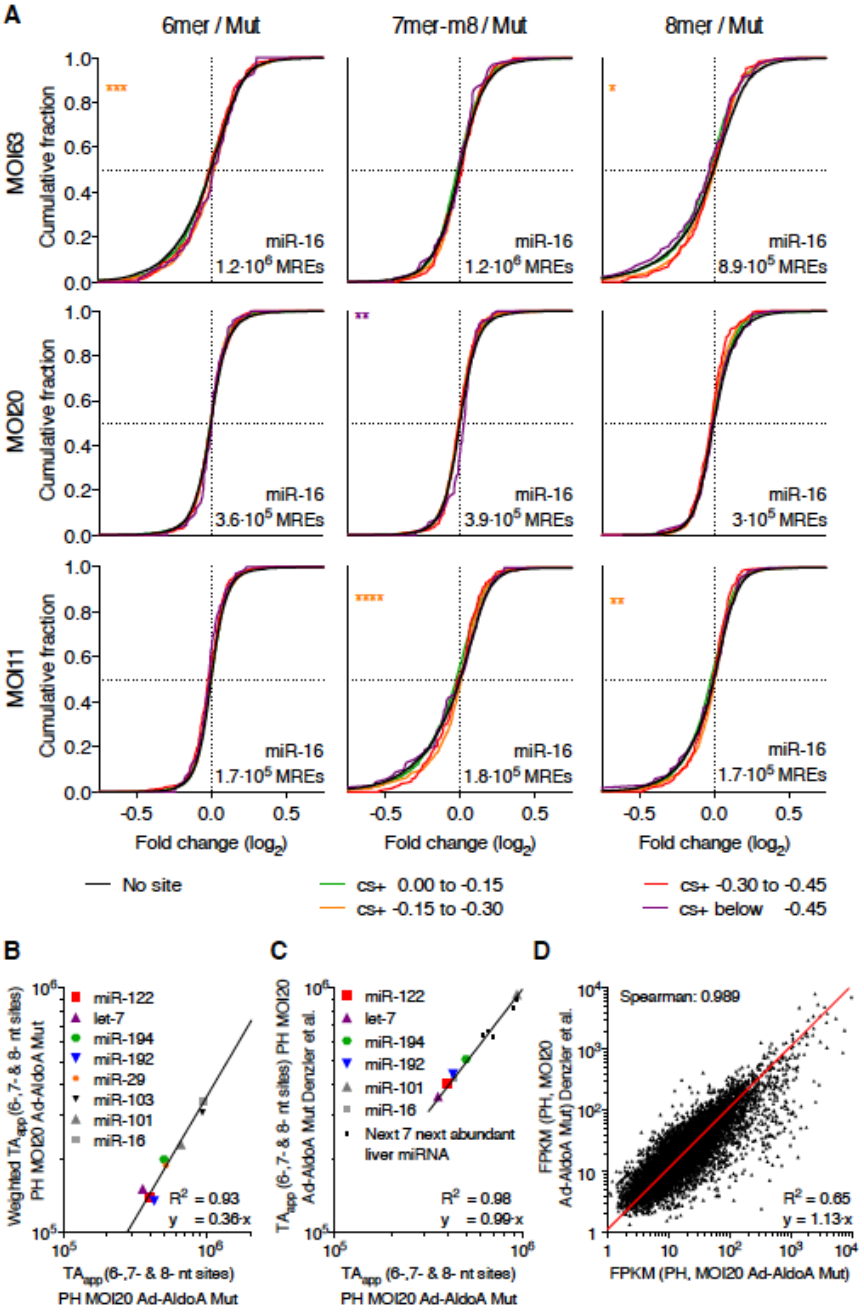

Figure S5. TA_{app} of Primary Hepatocytes Described in Denzler et al. (2014) Is Comparable to that of this Study. Related to Figure 5.

(A) RNA-seq results (n = 2) showing derepression of predicted targets from hepatocytes infected with MOI 11, MOI 20, or MOI 63 of Ad-AldoA miR-122 8mer, miR-122 7mer-m8, miR-122 6mer, or Mut shown in Figure 5E. CDF of mRNA changes for predicted target genes of miR-16 with the indicated cs+ bins (color) or for genes with no respective miRNA site (black). MREs per cell evaluated by absolute quantification of *AldoA* by qPCR are shown on each graph. *p < 0.05, **p < 0.01, ***p < 0.001, ****p < 0.0001, one-sided K–S test.

(B) Relationship between weighted TA_{app} and TA_{app} of primary hepatocytes (PH) infected with MOI 20 of Ad-AldoA Mut. Line represents linear regression of data points.

(C and D) Relationship between RNA-seq data from this study and of published work (Denzler et al., 2014). Comparison of transcriptome TA_{app} (A) and FPKM (B) of primary hepatocytes (PH) infected with MOI 20 of Ad-AldoA Mut. Line represents linear regression of data points.

Figure S6
Denzler et al.

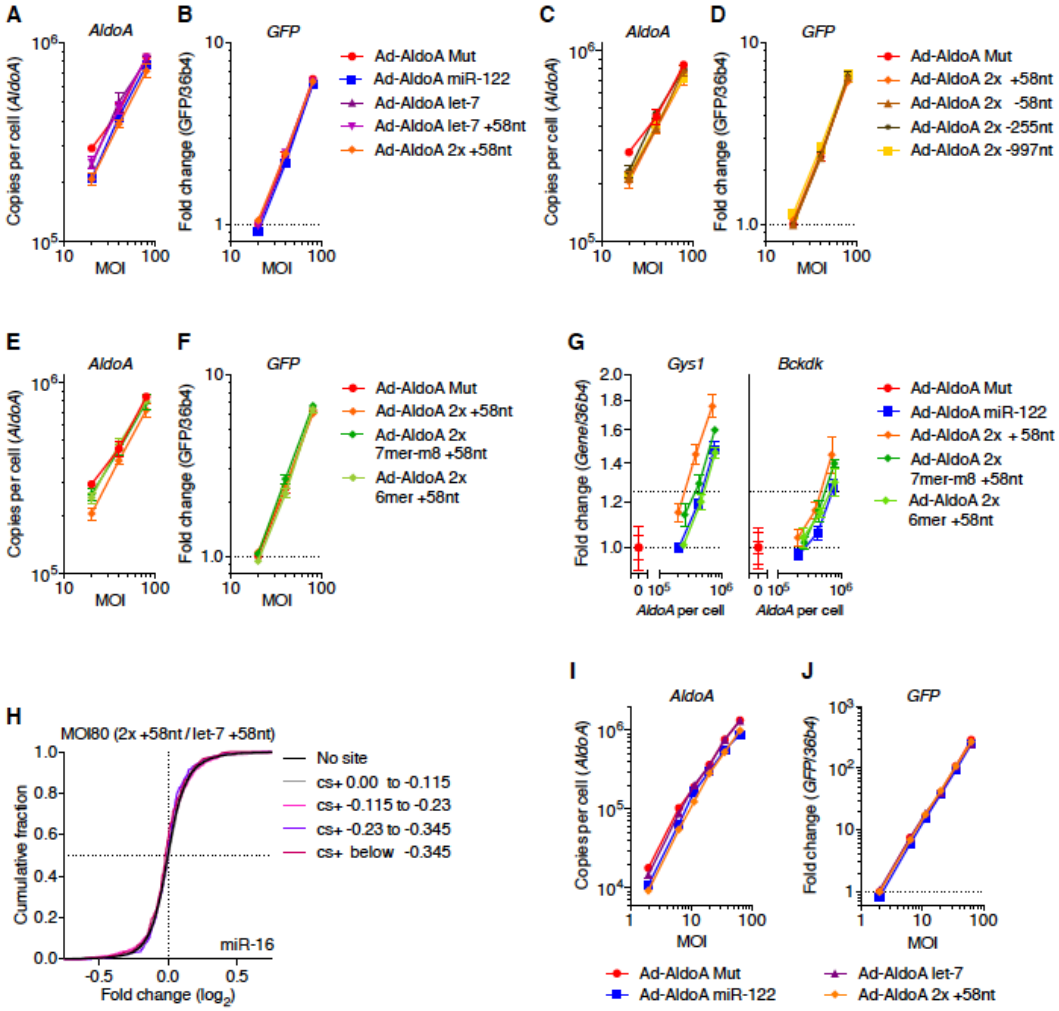

Figure S6. Overview of Ad-AldoA Constructs Harboring Seed Matches for Two Different miRNA Families. Related to Figure 6.

(A–J) Primary hepatocytes infected with different MOIs of Ad-AldoA Mut, miR-122, let-7, let-7 +58nt, 2x +58nt, 2x -58nt, 2x -255nt, 2x -997nt, 2x 7mer-m8 +58nt, or 2x 6mer +58nt. Absolute copy numbers per cell of *AldoA* (A, C, E, I), relative gene expression of *GFP* (B, D, F, J), and relative gene expression of miR-122 target genes (G). *GFP* are relative to Ad-AldoA Mut at the lowest MOI. Data represent mean ± SEM (n = 4). (H) RNA-seq results (n = 2) showing derepression of predicted targets from hepatocytes infected with MOI 80 of Ad-AldoA let-7 +58nt or 2x +58nt shown in Figure 6J. CDF of mRNA changes for predicted target genes of miR-16 with the indicated cs+ bins (color) or for genes with no respective miRNA site (black). MREs per cell evaluated by absolute quantification of *AldoA* by qPCR are shown on each graph. *p < 0.05, **p < 0.01, ***p < 0.001, ****p < 0.0001, one-sided K–S test.

Figure S7
Denzler et al.

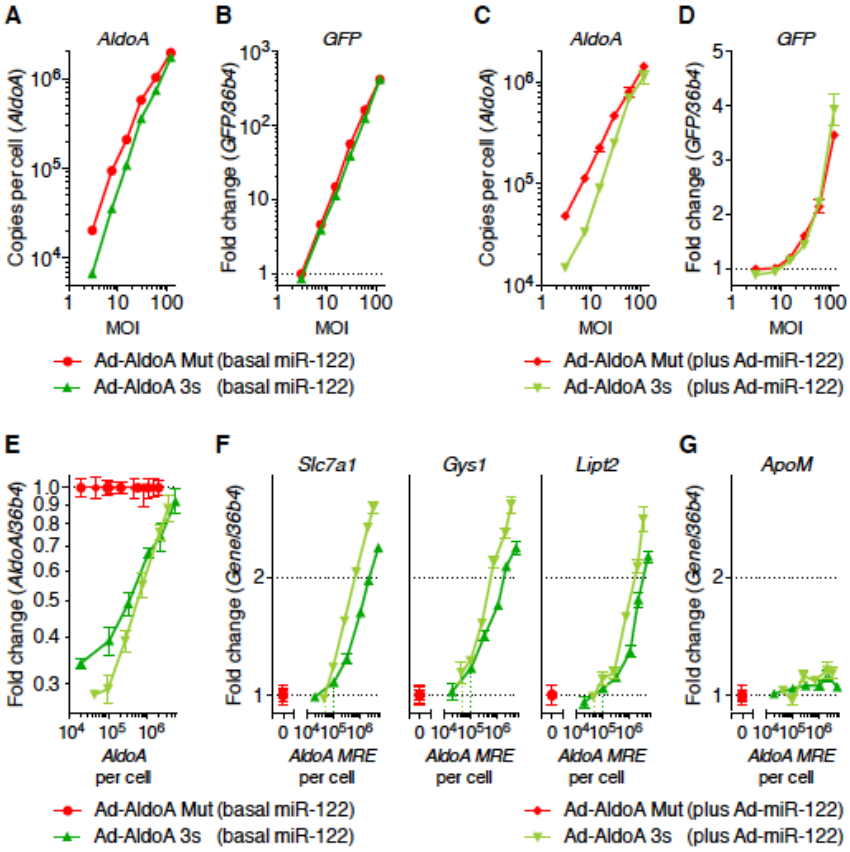

Figure S7. Derepression Is Enhanced when Mediated by Closely Spaced MREs of the Same miRNA Family. Related to Figure 3.

(A–G) Primary hepatocytes infected with different MOIs of Ad-AldoA Mut or 3s (n = 4) at basal miR-122 levels (A, B, and E–G), or in addition to MOI 50 of Ad-miR-122 (C–G). Absolute copy numbers per cell of *AldoA* (A, C), relative gene expression of *GFP* (B, D), *AldoA* (E), miR-122 target genes (F) or a control non-target gene (*ApoM*) (G). Data represent mean ± SEM (n = 4) for all panels.

Table S1: Gene Expression Levels, Fold Changes, and Predicted Target Site Efficacy Scores (context+ scores) across all Embryonic Stem Cell RNA-seq Samples. Related to Figures 1 and S1.

Table S2: miRNA Counts and RPM of Embryonic Stem Cells and Primary Hepatocyte Small RNA-seq Samples. Related to Figures 1, 4, S1 and S4.

Table S3: Gene Expression Levels, Fold Changes, and Predicted Target Site Efficacy Scores (context+ scores) across all Primary Hepatocyte RNA-seq Samples. Related to Figures 4, 5, 6, S4, S5, and S6.

Table S4: Primer Sets, siRNA and Northern Blot Probes Used in this Study. Related to Figures 1, 3, 4, 5, 6, S1, S3, S4, S5, S6, and S7.

Name	Sequence (5' to 3')
36b4 f	GCCGTGATGCCCAGGGAAGACA
36b4 r	CATCTGCTTGGAGCCCACGTTG
ApoM f	CCCAGACATGAAAACAGACCT
ApoM r	GGGTGTGGTGACCGATTG
AldoA f	GCGCTGTGTGCTAAAGATTG
AldoA r	AGGCTCCACAATGGGTACAA
Crot f	AGTGAAGGGCATTGTCCAAC
Crot r	TCTTGTGGATATATGTCAATTGTCTG
mCherry f	GCGTGATGAACTTCGAGGA
mCherry r	GATGAACTCGCCGTCCTG
eYFP f	GGACTGGTAGCTCAGGTAGTGG
eYFP r	CAGCAGAACACCCCCATC
GFP f	CACTACCTGAGCACCCAGTC
GFP r	TTGTACAGCTCGTCCATGCC
Gys1 f	GGTGTGAGGACGCAGGTAG
Gys1 r	GCCAACGCCCAAAATACA
Slc7a1 f	ATTTCAGCCGGCCTCCTA
Slc7a1 r	TGCCCACAGTGTCCCTTC
P4ha1 f	CGTGGGGAGGGTATCAAAAT
P4ha1 r	ATGGTAGCGGCAGAACAGTC
Ndrg3 f	TCCTGGCCAACAAGAAGC
Ndrg3 r	CTCATCCATGGTGGGGTACT
Tmed3 f	GGTCACGGCTCTCACTCAG
Tmed3 r	TCACAGTCTTCAGAGCCTCGT
Bckdk f	GAGAAGTGGGTGGATTTTGC
Bckdk r	ATGGGAATGAAGGGGAACC
Lipt2 f	CCCTACACTGGCGTCTGG
Lipt2 r	CATGTGAGGTCGGTTGAACA
Tgfbr1 f	GCAGCTCCTCATCGTGTTG
Tgfbr1 r	AGAGGTGGCAGAAACACTGTAAT
Nr6a1 f	GCTTGCCAGAGATCCGATAC
Nr6a1 r	AGTGCAGCACCACCTTAAAGA
Cdc34 f	GGAAGGACCGCGAGTACA
Cdc34 r	AGTACTCGGCCAGCGTAGTG
Arid3a f	ACCATGGGGACTGGACCT
Arid3a r	GGTCCGCATCCAGTTCATA
Fzd6 f	TTAAGCGAAACCGCAAGC
Fzd6 r	TTGGAAATGACCTTCAGCCTA
Cln5 f	ACTACAAGCCCCGATTTGG
Cln5 r	ACGGCGTCATGCATAAGTTT
Lrrfip1 f	GGCCAAATGTGAGCAACAG
Lrrfip1 r	CCTTGTGTGACTCGATCTGC
Cldn1 f	ACTCCTTGCTGAATCTGAACAGT
Cldn1 r	GGACACAAAGATTGCGATCAG

Tmem161b f	CCACCGTTGGGTAGAGAGAG
Tmem161b r	GCAGGTGACTTCGCATCAT
Ppat f	CTAGATGTGCCGCATGTGAT
Ppat r	AATACCAGCGCTCTCCTGAC
Klf9 f	CTCCGAAAAGAGGCACAAGT
Klf9 r	GCGAGAACTTTTTAAGGCAGTC
Ncbp2 f	TAAGGAGGGCAGGCAGTATG
Ncbp2 r	TTTTGTGCCAGTTTCCCATAG
Northern probe miR-122	CAAACACCATTGTCACACTCCA
Northern probe miR-16	CGCCAATATTTACGTGCTGCTA
Northern probe U6	CTCTGTATCGTTCCAATTTTAGTATA
miR-293 mimic	AGUGCCGCAGAGUUUGUAGUGU
miR-92a mimic	UAUUGCACUUGUCCCGGCCUG
miR-122 mimic	UGGAGUGUGACAAUGGUGUUUG
let-7f mimic	UGAGGUAGUAGAUUGUAUAGUU
Negative control siRNA 1	UGGUUUACAUGUCGACUAA
Negative control siRNA 2	UGGUUUACAUGUUGUGUGA
Negative control siRNA 3	UGGUUUACAUGUUUUCUGA
Negative control siRNA 4	UGGUUUACAUGUUUUCCUA

Table S5: 3′ UTR Sequences of Adenovirus Constructs that Harbor miRNA-Binding Sites After the Endogenous Stop Codon of AldoA.
Related to Figures 4, 5, 6, S4, S5, S6, and S7

All relevant miRNA-binding sites are highlighted in bold and colored by miRNA family: miR-122 (blue), let-7 (purple), miR-101 (grey), miR-194 (green), miR-192 (light blue), and mutated control (red). Emphasized in bold are the start codon, and the naturally occurring (TAA) or artificially introduced (TGA) stop codon. Underlined text shows translated polypeptide. The three stars indicate where the endogenous 3′ UTR of AldolaseA variant 2 starts.

Construct name	Sequence (5' to 3')
Shared sequence for all Ad-AldoA viruses shown in this table	CAGCTGAATAGGCTGCGTTCTCTTGGAACGCGCAGCAGAACGAGGTTCTGGTGACCCTAGCCGCGTTC GCTCCTTAGTCCTTTCGCCTACCCACCGGCGTACCAGGCAGACCCACCCCGTCCTGTGCCAGGAAAGC ACTGCCACCGGCACC**ATG**CCCCACCCATACCCAGCACTGACC**TGA**GAGCAGAAGAAGGAGCTGTCTGA CATCGCTCACCGCATTGTGGCTCCGGGCAAGGGCATCCTGGCTGCAGATGAGTCCACCGGAAGCATTG CCAAGCGCCTGCAGTCCATTGGCACCGAGAACACCGAGGAGAACAGGCGCTTCTACCGCCAGCTGCTG CTGACTGCAGACGACCGTGTGAATCCCTGCATTGGGGGGGTGATCCTCTTCCACGAGACACTGTACCA GAAGGCAGATGATGGACGTCCCTTCCCCCAAGTTATCAAGTCCAAGGGTGGTGTTGTGGGCATTAAGG TAGATAAGGGTGTGGTGCCCCTGGCAGGAACCAATGGCGAGACAACTACCCAGGGGCTGGATGGGCTG TCTGAACGCTGTGCCCAGTATAAGAAGGATGGAGCCGACTTTGCCAAGTGGCGCTGTGTGCTAAAGAT TGGGGAACATACTCCCTCGGCCCTGGCCATCATGGAAAATGCCAATGTTCTGGCCCGTTATGCCAGCA TCTGCCAGCAGAATGGCATTGTACCCATTGTGGAGCCTGAAATTCTCCCTGATGGGGACCATGACTTG AAGCGCTGCCAGTATGTTACTGAGAAGGTCCTGGCGGCTGTCTACAAGGCTCTGAGCGACCACCATGT CTATCTGGAAGGCACATTGCTGAAGCCCAACATGGTCACCCCTGGCCATGCTTGCACCCAGAAATTTT CCAATGAGGAGATTGCCATGGCAACGGTCACAGCACTTCGTCGCACAGTGCCCCCTGCTGTCACTGGG GTCACTTTCCTGTCTGGAGGGCAGAGTGAGGAAGAGGCATCCATCAACCTCAATGCTATCAACAAGTG CCCCCTGCTGAAGCCATGGGCCTTGACTTTCTCCTATGGTCGAGCCCTGCAGGCCTCTGCTCTAAAGG CCTGGGGTGGGAAGAAGGAGAACCTGAAGGCAGCCCAGGAGGAGTACATCAAGCGCGCCCTGGCCAAC AGCCTCGCTTGTCAAGGAAAGTATACCCCAAGTGGCCAGTCTGGAGCCGCAGCCAGTGAATCTCTCTT CATCTCTAACCATGCCTAC**TAA*****

Ad-AldoA Mut	**TAA*****CCAGAGCTGAACTAAGGCTGCTCCATCA**ACCATAAA**CGCGTCTGCCTACCCACTTGCTATTG AAGAGGGGTCTTCAGGCTCTTTCCCATCACTCTTGCTGCTGCCCTCGTGTGCGGTGTTGTCTGTGAAT GCTAAATCTGCCATCCCTTCCAGCCCACTGCCAATAAACAACTATTTAAGGGGGAAAAAAA
Ad-AldoA miR-122 (8mer)	**TAA*****CCAGAGCTGAACTAAGGCTGCTCCATCA**ACACTCCA**CGCGTCTGCCTACCCACTTGCTATTG AAGAGGGGTCTTCAGGCTCTTTCCCATCACTCTTGCTGCTGCCCTCGTGTGCGGTGTTGTCTGTGAAT GCTAAATCTGCCATCCCTTCCAGCCCACTGCCAATAAACAACTATTTAAGGGGGAAAAAAA
Ad-AldoA miR-122 (7mer-m8)	**TAA*****CCAGAGCTGAACTAAGGCTGCTCCATCA**ACACTCC**TCGCGTCTGCCTACCCACTTGCTATTG AAGAGGGGTCTTCAGGCTCTTTCCCATCACTCTTGCTGCTGCCCTCGTGTGCGGTGTTGTCTGTGAAT GCTAAATCTGCCATCCCTTCCAGCCCACTGCCAATAAACAACTATTTAAGGGGGAAAAAAA
Ad-AldoA miR-122 (6mer)	**TAA*****CCAGAGCTGAACTAAGGCTGCTCCATCAT**CACTCC**TCGCGTCTGCCTACCCACTTGCTATTG AAGAGGGGTCTTCAGGCTCTTTCCCATCACTCTTGCTGCTGCCCTCGTGTGCGGTGTTGTCTGTGAAT GCTAAATCTGCCATCCCTTCCAGCCCACTGCCAATAAACAACTATTTAAGGGGGAAAAAAA
Ad-AldoA 3s (miR-122)	**TAA*****CCAGAGCTGAACTAAGGCTGCTCCATCA**ACACTCCA**CGCGAGCTGCTCCATCA**ACACTCCA**C GCGAGCTGCTCCATCA**ACACTCCA**CGCGTCTGCCTACCCACTTGCTATTGAAGAGGGGTCTTCAGGCT CTTTCCCATCACTCTTGCTGCTGCCCTCGTGTGCGGTGTTGTCTGTGAATGCTAAATCTGCCATCCCT TCCAGCCCACTGCCAATAAACAACTATTTAAGGGGGAAAAAAA
Ad-AldoA bu4 (miR-122)	**TAA*****CCAGAGCTGAACTA**CAAACACCAT**ATCA**ACACTCCA**CGCGTCTGCCTACCCACTTGCTATTG AAGAGGGGTCTTCAGGCTCTTTCCCATCACTCTTGCTGCTGCCCTCGTGTGCGGTGTTGTCTGTGAAT GCTAAATCTGCCATCCCTTCCAGCCCACTGCCAATAAACAACTATTTAAGGGGGAAAAAAA
Ad-AldoA let-7	**TAA*****CCAGAGCTGAACTAAGGCTGCTCCATCA**CTACCTCA**CGCGTCTGCCTACCCACTTGCTATTG AAGAGGGGTCTTCAGGCTCTTTCCCATCACTCTTGCTGCTGCCCTCGTGTGCGGTGTTGTCTGTGAAT GCTAAATCTGCCATCCCTTCCAGCCCACTGCCAATAAACAACTATTTAAGGGGGAAAAAAA
Ad-AldoA let-7 +58nt	**TAA*****CCAGAGCTGAACTAAGGCTGCTCCATCA**ACCATAAA**CGCGTCTGCCTACCCACTTGCTATTG AAGAGGGGTCTTCAGGCTCTTTCCCATCACTC**CTACCTCA**GCCCTCGTGTGCGGTGTTGTCTGTGAAT GCTAAATCTGCCATCCCTTCCAGCCCACTGCCAATAAACAACTATTTAAGGGGGAAAAAAA
Ad-AldoA miR-101	**TAA*****CCAGAGCTGAACTAAGGCTGCTCCATCA**GTACTGTA**CGCGTCTGCCTACCCACTTGCTATTG AAGAGGGGTCTTCAGGCTCTTTCCCATCACTCTTGCTGCTGCCCTCGTGTGCGGTGTTGTCTGTGAAT GCTAAATCTGCCATCCCTTCCAGCCCACTGCCAATAAACAACTATTTAAGGGGGAAAAAAA
Ad-AldoA miR-194	**TAA*****CCAGAGCTGAACTAAGGCTGCTCCATCA**CTGTTACA**CGCGTCTGCCTACCCACTTGCTATTG AAGAGGGGTCTTCAGGCTCTTTCCCATCACTCTTGCTGCTGCCCTCGTGTGCGGTGTTGTCTGTGAAT GCTAAATCTGCCATCCCTTCCAGCCCACTGCCAATAAACAACTATTTAAGGGGGAAAAAAA
Ad-AldoA miR-192	**TAA*****CCAGAGCTGAACTAAGGCTGCTCCATCA**TAGGTCAA**CGCGTCTGCCTACCCACTTGCTATTG AAGAGGGGTCTTCAGGCTCTTTCCCATCACTCTTGCTGCTGCCCTCGTGTGCGGTGTTGTCTGTGAAT GCTAAATCTGCCATCCCTTCCAGCCCACTGCCAATAAACAACTATTTAAGGGGGAAAAAAA
Ad-AldoA 2x +58nt	**TAA*****CCAGAGCTGAACTAAGGCTGCTCCATCA**ACACTCCA**CGCGTCTGCCTACCCACTTGCTATTG AAGAGGGGTCTTCAGGCTCTTTCCCATCACTC**CTACCTCA**GCCCTCGTGTGCGGTGTTGTCTGTGAAT GCTAAATCTGCCATCCCTTCCAGCCCACTGCCAATAAACAACTATTTAAGGGGGAAAAAAA
Ad-AldoA 2x 7mer-m8 +58nt	**TAA*****CCAGAGCTGAACTAAGGCTGCTCCATCA**ACACTCC**TCGCGTCTGCCTACCCACTTGCTATTG AAGAGGGGTCTTCAGGCTCTTTCCCATCACTC**CTACCTCA**GCCCTCGTGTGCGGTGTTGTCTGTGAAT GCTAAATCTGCCATCCCTTCCAGCCCACTGCCAATAAACAACTATTTAAGGGGGAAAAAAA
Ad-AldoA 2x 6mer +58nt	**TAA*****CCAGAGCTGAACTAAGGCTGCTCCATCAT**CACTCC**TCGCGTCTGCCTACCCACTTGCTATTG AAGAGGGGTCTTCAGGCTCTTTCCCATCACTC**CTACCTCA**GCCCTCGTGTGCGGTGTTGTCTGTGAAT GCTAAATCTGCCATCCCTTCCAGCCCACTGCCAATAAACAACTATTTAAGGGGGAAAAAAA

Table S6: 3′ UTR Sequences of Adenovirus Constructs that Harbor a miRNA-Site Before the Endogenous Stop Codon of AldoA. Related to Figures 6 and S6.

In bold and colors are miR-122 (blue) and let-7 (purple) binding sites, emphasized in bold are the start codon, and the naturally occurring (TAA) or artificially introduced (TGA) stop codon. Underlined text shows translated polypeptide. The three stars indicate where the endogenous 3′ UTR of AldolaseA variant 2 starts.

Construct name	Sequence (5' to 3')
Ad-AldoA 2x -58nt	CAGCTGAATAGGCTGCGTTCTCTTGGAACGCGCAGCAGAACGAGGTTCTGGTGACCCTAGCCGCGTTCG CTCCTTAGTCCTTTCGCCTACCCACCGGCGTACCAGGCAGACCCACCCCGTCCTGTGCCAGGAAAGCAC TGCCACCGGCACC**ATG**CCCCACCCATACCCAGCACTGACC**TGA**GAGCAGAAGAAGGAGCTGTCTGACAT CGCTCACCGCATTGTGGCTCCGGGCAAGGGCATCCTGGCTGCAGATGAGTCCACCGGAAGCATTGCCAA GCGCCTGCAGTCCATTGGCACCGAGAACACCGAGGAGAACAGGCGCTTCTACCGCCAGCTGCTGCTGAC TGCAGACGACCGTGTGAATCCCTGCATTGGGGGGGTGATCCTCTTCCACGAGACACTGTACCAGAAGGC AGATGATGGACGTCCCTTCCCCCAAGTTATCAAGTCCAAGGGTGGTGTTGTGGGCATTAAGGTAGATAA GGGTGTGGTGCCCCTGGCAGGAACCAATGGCGAGACAACTACCCAGGGGCTGGATGGGCTGTCTGAACG CTGTGCCCAGTATAAGAAGGATGGAGCCGACTTTGCCAAGTGGCGCTGTGTGCTAAAGATTGGGGAACA TACTCCCTCGGCCCTGGCCATCATGGAAAATGCCAATGTTCTGGCCCGTTATGCCAGCATCTGCCAGCA GAATGGCATTGTACCCATTGTGGAGCCTGAAATTCTCCCTGATGGGGACCATGACTTGAAGCGCTGCCA GTATGTTACTGAGAAGGTCCTGGCGGCTGTCTACAAGGCTCTGAGCGACCACCATGTCTATCTGGAAGG CACATTGCTGAAGCCCAACATGGTCACCCCTGGCCATGCTTGCACCCAGAAATTTTCCAATGAGGAGAT TGCCATGGCAACGGTCACAGCACTTCGTCGCACAGTGCCCCCTGCTGTCACTGGGGTCACTTTCCTGTC TGGAGGGCAGAGTGAGGAAGAGGCATCCATCAACCTCAATGCTATCAACAAGTGCCCCCTGCTGAAGCC ATGGGCCTTGACTTTCTCCTATGGTCGAGCCCTGCAGGCCTCTGCTCTAAAGGCCTGGGGTGGGAAGAA GGAGAACCTGAAGGCAGCCCAGGAGGAGTACATCAAGCGCGCCCTGGCCAACAGCCTCGCTTGTCAAGG AAAGTATACCCCAAGTGGCCAGTCTGGAGCCGCAG**CTACCTCA**TCTCTCTTCATCTCTAACCATGCCTA C**TAA*****CCAGAGCTGAACTAAGGCTGCTCCATCA**ACACTCCA**CGCGTCTGCCTACCCACTTGCTATTG AAGAGGGGTCTTCAGGCTCTTTCCCATCACTCTTGCTGCTGCCCTCGTGTGCGGTGTTGTCTGTGAATG CTAAATCTGCCATCCCTTCCAGCCCACTGCCAATAAACAACTATTTAAGGGGGAAAAAAA
Ad-AldoA 2x -255nt	CAGCTGAATAGGCTGCGTTCTCTTGGAACGCGCAGCAGAACGAGGTTCTGGTGACCCTAGCCGCGTTCG CTCCTTAGTCCTTTCGCCTACCCACCGGCGTACCAGGCAGACCCACCCCGTCCTGTGCCAGGAAAGCAC TGCCACCGGCACC**ATG**CCCCACCCATACCCAGCACTGACC**TGA**GAGCAGAAGAAGGAGCTGTCTGACAT CGCTCACCGCATTGTGGCTCCGGGCAAGGGCATCCTGGCTGCAGATGAGTCCACCGGAAGCATTGCCAA GCGCCTGCAGTCCATTGGCACCGAGAACACCGAGGAGAACAGGCGCTTCTACCGCCAGCTGCTGCTGAC TGCAGACGACCGTGTGAATCCCTGCATTGGGGGGGTGATCCTCTTCCACGAGACACTGTACCAGAAGGC AGATGATGGACGTCCCTTCCCCCAAGTTATCAAGTCCAAGGGTGGTGTTGTGGGCATTAAGGTAGATAA GGGTGTGGTGCCCCTGGCAGGAACCAATGGCGAGACAACTACCCAGGGGCTGGATGGGCTGTCTGAACG CTGTGCCCAGTATAAGAAGGATGGAGCCGACTTTGCCAAGTGGCGCTGTGTGCTAAAGATTGGGGAACA TACTCCCTCGGCCCTGGCCATCATGGAAAATGCCAATGTTCTGGCCCGTTATGCCAGCATCTGCCAGCA GAATGGCATTGTACCCATTGTGGAGCCTGAAATTCTCCCTGATGGGGACCATGACTTGAAGCGCTGCCA GTATGTTACTGAGAAGGTCCTGGCGGCTGTCTACAAGGCTCTGAGCGACCACCATGTCTATCTGGAAGG CACATTGCTGAAGCCCAACATGGTCACCCCTGGCCATGCTTGCACCCAGAAATTTTCCAATGAGGAGAT TGCCATGGCAACGGTCACAGCACTTCGTCGCACAGTGCCCCCTGCTGTCACTGGGGTCACTTTCCTGTC TGGAGGGCAGAGTGAGGAAGAGGCATCCATCAACCTCAATGCTAT**CTACCTCA**GCCCCCTGCTGAAGCC ATGGGCCTTGACTTTCTCCTATGGTCGAGCCCTGCAGGCCTCTGCTCTAAAGGCCTGGGGTGGGAAGAA GGAGAACCTGAAGGCAGCCCAGGAGGAGTACATCAAGCGCGCCCTGGCCAACAGCCTCGCTTGTCAAGG AAAGTATACCCCAAGTGGCCAGTCTGGAGCCGCAGCCAGTGAATCTCTCTTCATCTCTAACCATGCCTA C**TAA*****CCAGAGCTGAACTAAGGCTGCTCCATCA**ACACTCCA**CGCGTCTGCCTACCCACTTGCTATTG AAGAGGGGTCTTCAGGCTCTTTCCCATCACTCTTGCTGCTGCCCTCGTGTGCGGTGTTGTCTGTGAATG CTAAATCTGCCATCCCTTCCAGCCCACTGCCAATAAACAACTATTTAAGGGGGAAAAAAA
Ad-AldoA 2x -997nt	CAGCTGAATAGGCTGCGTTCTCTTGGAACGCGCAGCAGAACGAGGTTCTGGTGACCCTAGCCGCGTTCG CTCCTTAGTCCTTTCGCCTACCCACCGGCGTACCAGGCAGACCCACCCCGTCCTGTGCCAGGAAAGCAC TGCCACCGGCACC**ATG**CCCCACCCATACCCAGCACTGACC**TGA**GAGCAGAAGAAGGAGCTGTCTGACAT CGCTCACCGCATTGTGGCTCCGGGCAAGGGCATCCTGGCTGCAGATGAGTCCACCGGAAGCA**CTACCTC** **A**CGCCTGCAGTCCATTGGCACCGAGAACACCGAGGAGAACAGGCGCTTCTACCGCCAGCTGCTGCTGAC TGCAGACGACCGTGTGAATCCCTGCATTGGGGGGGTGATCCTCTTCCACGAGACACTGTACCAGAAGGC AGATGATGGACGTCCCTTCCCCCAAGTTATCAAGTCCAAGGGTGGTGTTGTGGGCATTAAGGTAGATAA GGGTGTGGTGCCCCTGGCAGGAACCAATGGCGAGACAACTACCCAGGGGCTGGATGGGCTGTCTGAACG CTGTGCCCAGTATAAGAAGGATGGAGCCGACTTTGCCAAGTGGCGCTGTGTGCTAAAGATTGGGGAACA TACTCCCTCGGCCCTGGCCATCATGGAAAATGCCAATGTTCTGGCCCGTTATGCCAGCATCTGCCAGCA GAATGGCATTGTACCCATTGTGGAGCCTGAAATTCTCCCTGATGGGGACCATGACTTGAAGCGCTGCCA GTATGTTACTGAGAAGGTCCTGGCGGCTGTCTACAAGGCTCTGAGCGACCACCATGTCTATCTGGAAGG CACATTGCTGAAGCCCAACATGGTCACCCCTGGCCATGCTTGCACCCAGAAATTTTCCAATGAGGAGAT TGCCATGGCAACGGTCACAGCACTTCGTCGCACAGTGCCCCCTGCTGTCACTGGGGTCACTTTCCTGTC TGGAGGGCAGAGTGAGGAAGAGGCATCCATCAACCTCAATGCTATCAACAAGTGCCCCCTGCTGAAGCC ATGGGCCTTGACTTTCTCCTATGGTCGAGCCCTGCAGGCCTCTGCTCTAAAGGCCTGGGGTGGGAAGAA GGAGAACCTGAAGGCAGCCCAGGAGGAGTACATCAAGCGCGCCCTGGCCAACAGCCTCGCTTGTCAAGG AAAGTATACCCCAAGTGGCCAGTCTGGAGCCGCAGCCAGTGAATCTCTCTTCATCTCTAACCATGCCTA C**TAA*****CCAGAGCTGAACTAAGGCTGCTCCATCA**ACACTCCA**CGCGTCTGCCTACCCACTTGCTATTG AAGAGGGGTCTTCAGGCTCTTTCCCATCACTCTTGCTGCTGCCCTCGTGTGCGGTGTTGTCTGTGAATG CTAAATCTGCCATCCCTTCCAGCCCACTGCCAATAAACAACTATTTAAGGGGGAAAAAAA

EXTENDED EXPERIMENTAL PROCEDURES

Fluorescent Reporter Plasmids

The reporter plasmids are based on the pTRE-Tight-BI (Clontech) and rtTA plasmid system, where a bidirectional Tet promoter expresses enhanced yellow fluorescent protein (eYFP) and mCherry (pTRE-Tight-BI mCherry/eYFP) that contain a nuclear localization signal (Mukherji et al., 2011). The 3′ UTR of *mCherry* contains either zero (0s), one (1s), or three consecutive (3s) 48 nucleotide-long-sequence stretches, which are comprised of one 8mer miRNA recognition element (MRE) and ±20 bp flanking regions (MRE-reporter-sequence). The flanking regions originate from sequences 20 bp up- and down-stream of the 8mer seed match of miR-293 in the mouse *Sirt7* 3′ UTR region(Bosson et al., 2014). rtTA, pWhitescript , pTRE-Tight-BI mCherry/eYFP 0s and three 3s reporter plasmids (for miR-293, mir-294 and miR-92) were attained from the Philipp Sharp laboratory. Reporter plasmids for miR-293 (1s), miR-294 (1s), miR-92 (1s), miR-16 (3s), miR-26 (3s) and miR-292-5p (3s) were created by cloning either one or three MRE-reporter-sequence(s) into pTRE-Tight-BI mCherry/eYFP 0s using the restriction sites HindIII and SalI (NEB) (Bosson et al., 2014). All reporter plasmid sequences were confirmed by Sanger sequencing.

Embryonic Stem Cell Culturing and Transfection

The male embryonic stem cell line E14 (from Prof. Constance Ciaudo laboratory) derived from 129/Ola mice was cultured in ESC media [DMEM 4.5 g/l glucose (Life Technologies), containing 15% heat-inactivated fetal bovine serum (Life Technologies), 1000 U/ml recombinant mouse LIF (Amsbio), 0.1 mM 2-mercaptoethanol (Sigma), 1% Penicillin-Streptomycin (Life Technologies), 1% Glutamax (Life Technologies), and 1mM sodium pyruvate (Life Technologies)] on a 0.1% gelatin-coated plated in the absence of feeder cells. For transfection, plates with ~80% confluence were trypsinized and plated at 2 x 10^5 cells/well in gelatin-coated Nucleon Delta Surface 12-well plates (Thermo Scientific). 16 to 24 hours after plating, cells were transfected in Opti-MEM (Life Technologies) with 5 μl Lipofectamine 2000 (Life Technologies), together with 250 ng reporter plasmid, 250 ng rtTA plasmid, 1000 ng pWhitescript, and when applicable with miRNA mimics (Microsynth) or Antagomir-293 (Axolabs). Six hours after transfection the media was changed to ESC media containing 1ug/ml Doxycycline (Sigma), incubated for 18 hours, and then harvested for downstream flow cytometry analysis. All cells were incubated at 37°C in a humidified atmosphere containing 5% CO_2.

Flow Cytometry

E14 were transfected with reporter and rtTA plasmids and induced with doxycycline 6 hours post-transfection as described above. 24 hours after doxycycline induction cells were trypsinized (Life Technologies) for 60–75 seconds, neutralized with ESC media, spun down for 3 min with 200g at 4°C, washed once with 1 ml ice cold FACS buffer [PBS (Life Technologies) with 5% heat-inactivated fetal bovine serum (Life Technologies)], resuspended in 100-200ul FACS buffer and kept on ice for no longer than 4 hours. Just before analysis cells were passed through a 35 μm cell strainer (Corning). Samples were analyzed by counting 100,000 events per biological replica using a FACSAria IIIu flow cytometer (BD Biosciences) and an 85 μm nozzle. For sorting, 40,000 – 75,000 cells from 3 different gates (shown in Figure S1A) were collected simultaneously into three different 1.5 ml tubes and lysed with 1 ml peqGold TriFast immediately after the completion of the sort. Flowjo software version 10 was used to extract fluorescent values of eYFP and mCherry for each cell. eYFP and mCherry fluorescent values were corrected for autofluorescence by subtracting the mean background fluorescence plus two standard deviation from mock-transfected controls as described in Bosson et al. (2014). While subtracting only the mean background fluorescence would more correctly maintain the linear relationship between the fluorescence values of the two reporters at low levels of expression, we perform this background subtraction as described to maintain consistency with prior work. We have performed our analysis by subtracting either the mean (~28 for mCherry and ~18 for eYFP), or the mean plus two standard deviations (~200 for mCherry and ~180 for eYFP), and found no large difference between the curves generated nor our resulting interpretation. Cells with fluorescence values below 0 after background subtraction were excluded from further analyses. Data were log-transformed, divided into 20 bins based on eYFP level in the range of 10^3 – 1.25 x 10^5, and mean mCherry fluorescence values were calculated for each eYFP bin. For fold-change calculations all 3s reporter co-transfections have been normalized to the 0s control with the same respective Antagomir or miRNA concentration, but only one representative 0s control is shown in the Figures. Only fold-change values with mean mCherry expression above 0.8 x 10^3 are shown in Figures 1 and 2.

Animal Experiments

Animals were maintained on a 12-hour light/dark cycle under a controlled environment in a pathogen-free facility at the Institute for Molecular Systems Biology, ETH Zürich (Switzerland). All animal experiments were approved by the ethics committee of the Kantonale Veterinäramt Zürich.

Hepatocytes Isolation, Viral Infections and Transfections

All hepatocyte experiments were performed in primary cells derived from mouse livers. Hepatocyte isolation is based on the method described by Zhang et al. (2012) with modifications described in Denzler et al. (2014). Male 8- to 12-week-old C57BL/6N mice (Janvier) were anesthetized by intraperitoneal injection of 150 μl pentobarbital (Esconarkon US vet) pre-diluted 1:5 in PBS. The liver was perfused by cannulation of the caudal vena cava with the portal vein as a drain. The liver was perfused with pre-warmed Hank's Balanced Salt Solution (Life Technologies) containing 0.5 mM EGTA followed by pre-warmed digestion medium [DMEM 1 g/l glucose (Life Technologies) supplemented with 1% Penicillin-Streptomycin (Life Technologies), 15mM HEPES (Life Technologies) and 30 μg/ml Liberase TM Research Grade medium Thermolysin concentration (Roche)] each for four minutes with a flow rate of 3 ml min^{-1}. The liver was surgically removed, hepatocytes released into 10 ml digestion media by shaking and supplemented with 15 ml ice cold low glucose media [DMEM 1 g/l glucose (Life Technologies) supplemented with 1% Penicillin-Streptomycin (Life Technologies), 10% heat-inactivated fetal bovine serum (Sigma) and 1% Glutamax (Life Technologies)] and filtered through a 100 μm Cell Strainer (BD). The suspension was then washed three times with 25 ml of ice-cold low glucose media (50 g at 4°C for 2 min). Hepatocytes were counted and plated at 300,000 cells/well in surface-treated 6-well plates (Corning Primaria) in low glucose media. 4–6 hours after plating, cells were transfected with miRNA mimics (Microsynth) employing RNAiMAX (Life Technologies) or infected with adenovirus constructs in Hepatozyme media [HepatoZYME-SFM (Life Technologies) supplemented with 1% Penicillin-Streptomycin (Life Technologies), 1% Glutamax (Life Technologies)] and harvested 24 hours post infection. All cells were incubated at 37°C in a humidified atmosphere containing 5% CO_2.

miRNA Mimics and Antagomir-293

miRNA mimics and respective negative controls were synthesized by Microsynth with dTdT overhangs in the 3' end of the sense and antisense strand. The siRNA negative control is a pool of four oligonucleotide sequences (See Table S4). Antagomir-293 was ordered from Axolabs based on the following sequence/chemistry: ascsAfscsusascsAfsasascsuscsUfsgscsgsgscsascsu (2'-O-methyl-nucleotide: a, c, g, u; 2'-fluoro-nucleotide: Af, Cf, Gf, Uf; phosphorothionate: s)

Generation of Adenovirus Constructs

Recombinant adenoviruses generated in this study are either based on the *AldolaseA*-expressing adenovirus constructs (Ad-AldoA), described in Denzler et al. (2014), harboring either one (1s) or a mutated (Mut) miR-122 binding site, or express a miRNA precursor as described in Krützfeldt et al. (2005) and Krützfeldt et al. (2012). All adenoviruses were produced by Viraquest Inc., USA, employing the plasmid pVQAd CMV K-NpA. AldolaseA variant 2 (*AldoA*, NM_007438) with a translational stop codon at amino acid residue ten and a MluI restriction site after the endogenous (1s) or mutated (Mut) miR-122 binding site was introduced into pVQAd using the restriction sites BamHI and XhoI (NEB). All adenovirus constructs express green fluorescent protein (GFP) mRNA from an independent promoter. Nucleotide sequences of all Ad-AldoA constructs used in this study were confirmed by Sanger sequencing and are shown in Tables S5 and S6.

RNA Isolation

RNA was extracted using TRI Reagent (Sigma) or peqGold TriFast (Peqlab) according to the manufacturer's instructions, except for a 30 min isopropanol precipitation at –20°C.

RNA Amounts Per Cell

To determine per cell RNA amounts for ESCs, a confluent plate was trypsinized, the cells counted and 2 x 10^5 or 2 x 10^6 cells lysed in quadruplicates in 1 ml peqGold TriFast. Dividing the recovered RNA by the number of counted cells yielded 22.95 ± 0.25 pg/cell for ESCs. RNA measurements were transformed to per cell units either with 22.95 pg/cell for ESCs or with the previously published value of 73.5/cell for primary hepatocytes (Denzler et al., 2014).

Gene Expression Analysis

2 ug of total RNA was treated with the DNA-free Kit (Life Technologies) and reverse-transcribed using the High Capacity cDNA Reverse Transcription Kit (Life Technologies). Quantitative PCR reactions were performed with the Light Cycler 480 (Roche) employing a 384-well format, gene-specific primer pairs (see Table S4, designed by http://qpcr.probefinder.com/organism.jsp) and KAPA SYBR Fast qPCR Master Mix (2x) for LightCycler 480 (Kapa Biosystems). Cycles were quantified employing Light Cycler 480 Analysis Software (Abs quantification/ 2nd derivate max). Relative gene expression was calculated using the ddCT method and mouse *36b4* (*Rplp0*) for normalization. For absolute mRNA quantification of *AldoA*, *Crot* and

ApoM standard curves from Denzler et al. (2014) were taken, where plasmids were in vitro transcribed, reverse transcribed and used for a standard curve. For absolute quantification of *eYFP* and *mCherry*, a dilution series of *eYFP*, *mCherry* and containing plasmids were directly used in qPCR reactions to create standard curves, as *AldoA* standard curves derived directly from plasmids were similar that those retained through in vitro transcription. Molar concentrations of plasmids were quantified using a NanoDrop ND-1000 spectrophotometer (Thermo Scientific) and the respective molecular weight.

miRNA Expression Analysis

miRNA expression analysis was performed as previously described in Denzler et al. (2014). 240 ng of total RNA was reverse-transcribed using TaqMan MicroRNA Assays (Life Technologies) and TaqMan MicroRNA Reverse Transcription Kit (Life Technologies). The RT primers were multiplexed in a dilution of 1:20 as described by the manufacturer. To avoid quantification biases caused by similar miRNA sequences, miRNAs of the same seed family were not multiplexed in the same reaction. Quantitative PCR reactions were performed with the Light Cycler 480 (Roche) employing a 384-well format, TaqMan Universal PCR Master Mix, No AmpErase UNG (Life Technologies) and TaqMan MicroRNA Assays (Life Technologies). Cycles were quantified employing Light Cycler 480 analysis software (Abs quantification/ 2^{nd} derivate max). Relative miRNA expression was calculated using the ddCT method and mouse snoRNA202 for normalization. For absolute quantification synthetic miRNAs (Sigma-Aldrich) were quantified using a NanoDrop ND-1000 spectrophotometer (Thermo Scientific) and the respective molecular weight. miRNAs were spiked into primary hepatocyte cell lysates and absolutely quantified employing a synthetic miRNA standard curve. Absolute miRNA copy numbers of adenovirus-infected primary hepatocytes shown Figures S3A and S4M were calculated by multiplying relative abundances (miRNA/snoRNA202), which were normalized to uninfected hepatocytes, with the copy number evaluated in either Figure 4A or in Denzler et al. (2014)

Small RNA Sequencing and Data Analysis:

Total RNA was size fractionated (18–35 nt), followed by 5’ adapter (Truseq small RNA 5’ adapter RA5 + 8Ns, GUUCAGAGUUCUACAGUCCGACGAUCNNNNNNNN) and 3’ adapter (NNNNAGAUCGGAAGAGCACACGUCU/3ddC/) ligations, RT-PCR, and Solexa sequencing. To quantify miRNA levels, we counted the number of occurrences in which the first 20 nt of the raw sequence matched a known mature

Mus musculus miRNA sequence of miRBase version 20. All raw and processed data files have been deposited in GEO and can be found under the accession number GSE76288.

RNA-seq Data Analysis

To process RNA-seq data, we utilized the same general strategy described previously (Denzler et al., 2014). Briefly, raw reads were aligned to the latest build of the mouse genome (mm10) using STAR v. 2.3.1n (options --outFilterType BySJout --outFilterMultimapScoreRange 0 --readMatesLengthsIn Equal --outFilterIntronMotifs RemoveNoncanonicalUnannotated --clip3pAdapterSeq TCGTATGCCGTCTTCTGCTTG --outStd SAM (Dobin et al., 2013). Pooling all biological replicates of a particular sample, differential expression analysis was performed between two samples of interest using cuffdiff v. 2.1.1 (options --library-type fr-firststrand -b mm10.fa -u --max-bundle-frags 100000000) (Trapnell et al., 2013), using mouse transcript models of protein-coding and long noncoding RNA genes annotated in Ensembl release 72. All raw and processed data files have been deposited in GEO and can be found under the accession number GSE76288. For data analysis, only genes with FPKM above 2.0 (ESCs) or above 1.0 (primary hepatocytes) were considered. For cumulative distribution function calculations, fold change values (log2) were corrected for biases due to 3′ UTR length by fitting a linear model to mRNA fold change (log2) as a function of the 3′ UTR length of each respective transcript (see Tables S1 and S3), and subsequently subtracting the predicted model value for all transcripts.

Absolute Copy Numbers Evaluation from RNA-seq Data (ESCs)

We fit a linear regression function to transform gene expression measurements (measured in FPKM) from RNA-seq data into absolute copy numbers (as determined by quantitative PCR). The data was log-transformed and fit to a linear equation of the form Y = X + B, in which Y = log(y) and X = log(x). Fixing the slope to be 1 constrains the regression such that a linear relationship is maintained between the non-transformed values, x and y. Copy numbers per cell were determined by multiplying the FPKM by 10^B, in which B is the y-intercept from the fit linear regression. To transform published ESC RNA-seq data (Bosson et al., 2014) we fit a linear regression between log-transformed FPKM of published ESC data and FPKM from ESCs transfected with the 0s reporter and sorted for low eYFP expressing cells, with the same equation as above. Copy numbers per cell were then determined by multiplying the FPKM of published ESC data by the transformed y-intercept, 10^B.

Absolute Copy Number Evaluation from RNA-seq Data (Primary Hepatocytes)

To transform our primary hepatocyte data from this study to copies per cells we fit a linear regression function between log-transformed FPKM of published hepatocytes (Denzler et al., 2014), where copy numbers of sequencing data were known, and FPKM of primary hepatocytes from this study, with the same equation as described in the previous paragraph. Copy numbers per cell were then determined by multiplying the FPKM of published hepatocyte data by the transformed y-intercept, 10^B.

Small RNA Sequencing and Data Analysis:

Total RNA was size fractionated (18–35 nt), followed by ligation of 3' preadenylated adapter (AppNNNNAGATCGGAAGAGCACACGTCTddC) and 5' adapter (Truseq small RNA 5' adapter RA5 + 8Ns, GUUCAGAGUUCUACAGUCCGACGAUCNNNNNNNN), reverse transcription, PCR amplification, and Solexa sequencing. To quantify miRNA levels, we counted the number of occurrences in which the first 20 nt of the raw sequence matched a known mature Mus musculus miRNA sequence of miRBase version 20. All raw and processed data files have been deposited in GEO and can be found under the accession number GSE76288.

Target Abundance Calculation

For each miRNA, the copy number of each predicted target gene was multiplied with the number of 6-, 7-, and 8-nt 3′ UTR binding sites, and these values were summed to yield TA_{app}.

Northern Blotting

Northern blotting was performed as described in Title et al. (2015). 10 ug of RNA, were denatured and separated on a 15% denaturing polyacrylamide gel containing 7.5 M urea (SequaGel, National Diagnostics). Separated RNAs were then transferred onto a Hybond Nx nylon membrane (GE Healthcare Life Sciences) and cross-linked using 1-ethyl-3-(3-dimethylaminopropyl) carbodiimide (Thermo Scientific) as detailed by Pall and Hamilton (2008). miR-122 and miR-16 DNA oligonucleotide probes were designed as the reverse complement of the mature miRNA sequence or the U6 transcript (See Table S4). 20 pmol was labeled with [γ-^{32}P]dATP (PerkinElmer Life Sciences) using T4 polynucleotide kinase (NEB). Membranes were prehybridized at 50 °C under rotation for 1 h and hybridized with the labeled probe overnight (20 mM Na_2HPO_4 (pH 7.2), 7% SDS, 25% 20x SSC, 0.02% albumin, 0.02% polyvinyl-

pyrrolidon K30, 0.02% Ficoll 400, and 0.1 mg/ml sonicated salmon sperm), followed by washing twice with buffer 1 (25% 20x SSC, and 5% SDS) and once with buffer 2 (5% 20x SSC, and 1% SDS) and exposure to a phosphorimaging screen for 8 hours to O/N. Signal was detected using the FLA-7000 (FujiFilm). Membranes were stripped with boiled 0.1% SDS, shaking, twice for 20 minutes, and exposed for a minimum of 24 hours to verify loss of signal.

Calculation of IC_{50} values from dual-reporter experiments

To determine the abundance of competing sites at which the amount of miRNA-mediated repression has decreased to half of that observed in the absence of competing sites, IC_{50}, the 3s reporter data were fit to a modified Hill equation using non-linear least-squares. The following describes how this equation was generated, as well as the relationship between maximal and half-maximal miRNA-mediated repression.

The time evolution of the cellular abundance of an mRNA *x* can be described as

$$\frac{dx}{dt} = \alpha - \beta x \qquad [1.1]$$

where α is the rate of transcription, and β is the first-order rate constant for its degradation. We highlight that the β term is a simplification representing an average over a variety of states of the mRNA and corresponding degradation rates. To highlight this we refer to β as β_{app}.

By setting the left-hand-side of equation [1.1] to 0, we arrive at expressions for the steady-state abundance of both a site-containing mRNA *s* and the corresponding no-site containing mRNA s_0

$$s = \frac{\alpha}{\beta_{app}} \ , \qquad [1.2]$$

$$s_0 = \frac{\alpha}{\beta_{0,app}} \ . \qquad [1.3]$$

We make the assumption that miRNA effects do not interfere with the miRNA-independent degradation mechanisms represented by $\beta_{0,app}$, allowing us to write equation [1.2] as

$$s = \frac{\alpha}{\beta_{0,app} + \beta_{miR,app}} \ . \qquad [1.4]$$

Where $\beta_{miR,app}$ is the apparent rate constant for miRNA-mediated degradation.

The observed fractional repression ρ is therefore given by

$$\rho = \frac{s}{s_0} = \frac{1}{1+R} \ , \qquad [1.5]$$

where $R = \beta_{miR,app}/\beta_{0,app}$, and represents the normalized increase in degradation of *s* due to miRNA-mediated repression. In the regime of target-site excess, the effects of the miRNA will be distributed equally across the entire pool of target sites, and so *R* will scale inversely with the target site abundance (TA):

$$R \propto \frac{1}{\mathrm{TA}} \ . \qquad [1.6]$$

Therefore, in conditions of constant miRNA concentration, the value of *R* with added competitor abundance s_e is given by

$$R = R_0 \frac{\mathrm{TA}}{s_e + \mathrm{TA}} \ , \qquad [1.7]$$

where R_0 is the value of *R* in the absence of added competitor.

For the dual reporter experiments, we use a modified version of this equation accounting for a three-site containing reporter with cooperative spacing:

$$R_{3site} = R_0 \frac{\mathrm{TA}^n}{(3s_e)^n + \mathrm{TA}^n} \qquad [1.8]$$

where *n* is the Hill coefficient for cooperative binding. Substituting *R* from equation [1.8] into [1.5] and rearranging yields

$$\rho = \frac{(3s_e)^n + \mathrm{TA}^n}{(3s_e)^n + \mathrm{TA}^n(1+R_0)} \ , \qquad [1.9]$$

which was fit against the data of Figures 1, 2, and S2.

Setting $s_e = 0$ in equation [1.9] to generate ρ_0, the value of ρ in the absence of added competitor, and rearranging yields

$$R_0 = \frac{1-\rho_0}{\rho_0} \ . \qquad [1.10]$$

Half-maximal derepression ρ_{50} is given by setting $R = R_0/2$ in equation [1.5] and substituting R_0 from equation [1.10]

$$\rho_{50} = \frac{1}{1+\frac{1}{2}R_0} = \frac{2\rho_0}{\rho_0+1} \ . \qquad [1.11]$$

This relationship is also used to calculate IC_{50} values in mathematical simulations of miRNA competition.

For the dual-reporter experiments measuring *mCherry* derepression in ESCs, the depression threshold (DRT) was defined as the abundance of competing target at which the fractional repression is equal to 90% of its maximum:

$$\rho_{\mathrm{DRT}} = \left(\rho_0\right)^{9/10} \qquad [1.12]$$

For the qPCR experiments measuring endogenous miRNA target derepression in primary hepatocytes, we used a variant of equation [1.9] normalized to ρ_0

$$\rho_{\text{norm}} = \frac{\rho}{\rho_0} = 1 + \frac{(3s_e)^n R_0}{(3s_e)^n + \text{TA}^n\left(1 + R_0\right)} \ , \qquad [1.13]$$

which was fit against the data of Figure S7 for the AldoA 3-site construct. In case of data originating from 1-site AldoA constructs in Figures 3, 4, 5, and 6, equation [1.13] was used in which n was set to 1 and $3s_e$ was replaced with s_e. In addition, since the number of added *AldoA* MREs never reached a level sufficient to observe complete derepression, the R_0 parameter from equation [1.13] could not accurately be fit. This precludes the DRT calculation as performed with the dual reporter experiments. We therefore modified our definition of DRT for the qPCR experiments to represent the abundance of competing target at which endogenous target genes have been upregulated by 10%.

$$\rho_{\text{DRT}_{\text{qPCR}}} = 1.1 \qquad [1.14]$$

Due to the measurement noise associated with the derepression signal for weak targets, the DRT was calculated by the average DRT of the two genes exhibiting the largest derepression.

Mathematical modeling of miRNA-mediated repression

As done previously (Mukherji et al., 2011; Ala et al., 2013; Bosson et al., 2014; Jens and Rajewsky, 2015; Schmiedel et al., 2015), we constructed a system of differential equations describing the regulation of mRNA targets by a miRNA. The system was solved at steady-state to arrive at an equation relating the occupancy and repression of each mRNA to the abundance and binding affinity of each mRNA, as well as the activity and abundance of the miRNA. The model includes a miRNA-programmed silencing complex (hereafter referred to as "free miRNA") m, and an arbitrary number of distinct mRNA target site types (hereafter referred to as "sites") $\boldsymbol{s} = (s_1, s_2, \ldots, s_n)$. The free miRNA can reversibly bind each free site s_i to form the corresponding miRNA–site complex (hereafter referred to as "complex") c_i. The mRNA species belonging to c_i is then subject to increased (miRNA-mediated) degradation. The behavior of this model is described by a system of coupled first-order differential equations, where:

$$\frac{dm}{dt} = \alpha_m - \beta_m m + \sum_i \left[\left(\beta_c + \beta_i + k_i^- \right) c_i - k_i^+ s_i m \right] \ , \qquad [2.1]$$

and for each site–complex pair:

$$\frac{ds_i}{dt} = \alpha_i + \left(\beta_m + k_i^-\right)c_i - \left(\beta_i + k_i^+ m\right)s_i \ , \qquad [2.2]$$

$$\frac{dc_i}{dt} = k_i^+ m s_i - \left(\beta_i + \beta_m + \beta_c + k_i^-\right)c_i \ . \qquad [2.3]$$

Free miRNA *m* is generated at rate α_m and degraded due to dilution and decay with rate constant β_m. Similarly, each site s_i is generated at rate α_i and degraded with rate constant β_i. Each complex c_i is formed from the association of free miRNA *m* and site s_i with rate constant k_i^+, and is lost due to either complex dissociation with rate constant k_i^-, independent degradation of either the miRNA or the mRNA within the complex with rate constant β_i or β_m respectively, or miRNA-dependent degradation of the mRNA within the complex with rate constant β_c. Independent degradation of the miRNA within the complex regenerates the free site s_i, whereas independent or miRNA-dependent degradation of the mRNA within the complex regenerates the free miRNA *m.*

Setting the left-hand side of equations [2.2] and [2.3] to 0 yields the steady-state solutions for s_i and c_i

$$s_i = \frac{\alpha_i K_i}{\beta_i\left(K_i + mB_i\right)} \ , \qquad [2.4]$$

$$c_i = \frac{\alpha_i m}{\beta_i\left(K_i + mB_i\right)} \ , \qquad [2.5]$$

where

$$B_i = \frac{\beta_i + \beta_c}{\beta_i} \ , \qquad [2.6]$$

is the maximum miRNA activity, or the fold-difference in stability between the free and bound form of each site *i* due to repression, and

$$K_i = \frac{\beta_c + \beta_i + \beta_m + k_i^-}{k_i^+} \ , \qquad [2.7]$$

is the Michaelis constant giving the concentration of the free site s_i at which repression will be half that of the maximum miRNA activity. This is distinct from the experimentally determined IC_{50} value, which reports the amount of additional competing sites necessary to observe half the repression of a miRNA target site compared to the condition in which no competing sites are added.

Substituting equations [2.4] and [2.5] into equation [2.1] and setting the left-hand side to 0 rearranges to an implicit expression for the steady-state solution for *m*:

$$\frac{\alpha_m}{\beta_m} = m + \frac{1}{\beta_m}\sum_i \left[\frac{m\left(K_i k_i^+ - k_i^- - \beta_i - \beta_c\right)}{K_i + mB_i} \frac{\alpha_i}{\beta_i} \right] . \quad [2.8]$$

By first rearranging equation [2.7] to

$$K_i k_i^+ = k_i^- + \beta_i + \beta_c + \beta_m \ , \quad [2.9]$$

and using equation [2.9] to substitute for $K_i k_i^+$, equation [2.8], can be simplified to

$$M = m + \sum_i \frac{m}{K_i + mB_i} T_i \ , \quad [2.10]$$

where $M = \alpha_m / \beta_m$ is the total amount of miRNA in the system, and $T_i = \alpha_i / \beta_i$ is the total amount of site *i* in the absence of repression. The fractional occupancy θ_i and the fractional repression ρ_i of each site *i* are given by

$$\theta_i \equiv \frac{c_i}{c_i + s_i} = \frac{m}{m + K_i} \ , \quad [2.11]$$

$$\rho_i \equiv \frac{c_i + s_i}{T_i} = \frac{K_i + m}{K_i + mB_i} \ , \quad [2.12]$$

which allow equation [2.10] to be written as

$$M = m + \sum_i \theta_i \rho_i T_i \ , \quad [2.13]$$

or two alternative forms

$$M = m + \sum_i \theta_i T_i' \ , \quad [2.14]$$

where $T_i' = \rho_i T_i$ represents the total amount of site *i* (incorporating repression) and

$$M = m + \sum_i c_i \ , \quad [2.15]$$

which recovers the definition of total miRNA *M* as the sum of free miRNA *m* and all complexes c_i in which it is engaged.

We applied two simplifications to the model, for the ease of implementation. First, we assigned a single value of *B* to all sites within a particular simulation. While the value of B_i is expected to vary across genes inversely related to mRNA half-life, the occurrences of each site are spread over many distinct mRNA species, allowing reasonable approximation of maximal miRNA activity in a particular cell type by a single parameter value. Second, we approximated the Michaelis terms as:

$$K_i \approx \frac{k_i^-}{k_i^+} = K_{\mathrm{D},i} \ , \quad [2.16]$$

given that reported rates of complex dissociation for high-affinity sites (Salomon et al., 2015) vastly exceed decay rates inferred from median mRNA half-life (9 h) (Schwanhausser et al., 2011). With these two adjustments, the final form of the

modeled system in equation [2.13] is parameterized by the abundances of each molecular species, in addition to two steady-state parameters B and $K_{D,i}$. This had the advantage of being immediately applicable to the dual fluorescence experiments, for which rate constants are not directly known.

We simulated either the occupancy or repression of an arbitrary site j (with dissociation constant $K_{D,j}$) in the presence of a competitor site e (with abundance T_e' that was varied across simulations and dissociation constant $K_{D,e}$) in addition to the pool of endogenous sites $\boldsymbol{s}$ (each with known, invariant abundance T_i' and dissociation constant $K_{D,i}$) and a given value of maximal miRNA activity B by application of either equation [2.11],

$$\theta_j = \frac{m_e}{K_{D,j} + m_e} \qquad [2.17]$$

or equation [2.12]:

$$\rho_j = \frac{K_{D,j} + m_e}{K_{D,j} + m_e B} \qquad [2.18]$$

where m_e is determined by solving equation [2.13] updated to include site e:

$$M = m_e + \sum_i \frac{m_e}{K_{D,i} + m_e B} T_i + \frac{m_e}{K_{D,e} + m_e} T_e' \ , \qquad [2.19]$$

in which the values of T_i are found by rearranging equation [2.12]:

$$T_i = \rho_i^{-1} T_i' = \frac{m_0 B + K_{D,i}}{m_0 + K_{D,i}} T_i' \ , \qquad [2.20]$$

where m_0 is the abundance of free miRNA in the absence of competitor, found by solving equation [2.15] in the absence of site e:

$$M = m_0 + \sum_i \frac{m_0}{K_{D,i} + m_0} T_i' \ . \qquad [2.21]$$

When simulating the mixed-affinity model for miR-293 in ESCs, we assigned parameter values as follows:

1.) M was set to the cellular miRNA abundance (2.6×10^3 copies per cell, or cpc).

2.) B was set according to 3.9, based on the amount of repression observed for an 8-nt site in the absence of added sites (~20%).

3.) The paired values for site abundances (T'_1, T'_2, …, T'_n) and dissociation constants ($K_{D,1}$, $K_{D,2}$, …, $K_{D,n}$) were determined through a two-step procedure. In the first step, we first generated T' and K_D values representing four distinct site type categories (8-, 7-, 6-nt and low-affinity sites). We set the total number of 8-, 7-, and 6-nt sites T'_{8nt}, T'_{7nt}, and T'_{6nt} by taking the number of canonical 3′ UTR sites in the absence of added exogenous target (2.1×10^4 cpc) and apportioning them at a 1:6:9

ratio. The representative dissociation constant for the 8-nt site $K_{D,8nt}$ was drawn from single-molecule experiments (18 pM) (Salomon et al., 2015), with the $K_{D,7nt}$ and $K_{D,6nt}$ scaled by 2- and 5-fold, respectively, based on the relative efficacy of either site in competition (Figure 5). We modeled the contribution of low-affinity sites, i.e., noncanonical/background sites, by assigning the fourth site type a representative dissociation constant $K_{D,la}$ arbitrarily scaled 300-fold in comparison to the 8-nt site, and setting the abundance of this site type T'_{la} such that the simulated IC_{50} (the combined effect of all four endogenous site types) agreed with experimental observation (3.3 x 10^4 cpc). The four representative K_D values were converted from pM to cpc based on a cellular diameter of 10 μm (Hong et al., 2012) and a cytoplasmic volume of 40% (Bosson et al., 2014). In the second step, we generated 10^3, 10^3, 10^3, and 10^4 variants of each the four site types, respectively. Each site-type variant was assigned a dissociation constant $K_{D,i}$ by log-transforming a value sampled from a normal distribution with mean = exp(K_D) and standard deviation = 0.3 x exp(K_D), where K_D is set to the corresponding value from the first step ($K_{D,8nt}$, $K_{D,7nt}$, $K_{D,6nt}$, or $K_{D,la}$). The T'_i value for each site type variant was set to the corresponding T' value from the first step (T'_{8nt}, T'_{7nt}, and T'_{6nt}, or T'_{la}) divided by the number of variants generated for that site type. We note that the aggregate effect of the low-affinity sites could be modeled without knowing the precise affinities and abundances of these sites because choosing different affinities would have caused corresponding adjustments to the inferred abundances to reach the same effect. Therefore, although the abundances and affinities of these low-affinity sites were unknown, their influence on the experimentally determined IC_{50} values, and thus their aggregate contribution to effective target abundance, was robustly simulated.

All simulations were performed using R to solve for *m* for a range of concentrations of the competing target (1 x 10^2 – 1 x 10^5 cpc). Repression of *mCherry* as a function of *mCherry* (Figure 7A, left) or *eYFP* (Figure 7A, middle) abundance is shown by plotting ρ_j from equation [2.18] as a function of either T_j or T'_j, respectively. The fraction of *mCherry* unbound to miRNA as a function of *mCherry* abundance (Figure 7B) is given by 1 – θ_j from equation [2.17] as a function of T'_j. The model from Bosson et al. (Figure 7C, left) was implemented as previously described (Bosson et al., 2014) and the model from Jens & Rajewsky (Figure 7C, right) was adapted by multiplying each $K_{D,i}$ by R_{vol}, the ratio of cytoplasmic volume of ESCs to that of monocytes, and multiplying each T'_i by R_{TA}, the ratio of the TA_{app} value for miR-293 ESCs to that of miR-20a in monocytes. To observe these models with added low-affinity sites (Figure 7D), we added 10^4 site types, assigning each a $K_{D,i}$ value by log-

transforming a value sampled from a normal distribution with mean = exp(300 x $K_{D,8nt\ site}$) and standard deviation = 0.3 x exp(300 x $K_{D,8nt\ site}$). The abundance of each of the 10^4 sub-types was chosen such that the combined effect of these new sites and those originally present in either model resulted in an IC_{50} in agreement with experimental observation (3.3 x 10^4 cpc).

The IC_{50} for site occupancy (represented by a solid vertical line in Figures 7B, C, and D) is given by the abundance of competing site at which the fraction of that site (and all other sites with identical K_D) that is bound by miRNA is half of that modeled in the absence of competing sites:

$$M = m_{50,\theta} + \sum_i \frac{m_{50,\theta}}{K_{D,i} + m_{50,\theta} B} T + \frac{m_{50,\theta}}{K_{D,e} + m_{50,\theta}} \mathrm{IC}_{50,\theta} \ , \qquad [2.22]$$

where $m_{50,e}$ satisfies the relationship:

$$\theta_e(m_{50,\theta}) = \frac{1}{2}\theta_e(m_0) \ , \qquad [2.23]$$

such that

$$m_{50,\theta} = \frac{K_{D,i} m_0}{m_0 + 2K_{D,i}} \ . \qquad [2.24]$$

The IC_{50} for site repression (represented by a solid vertical line in both panels of Figure 7A) is given by the abundance of competing site *e* at which the apparent rate of miRNA-mediated degradation of the target has decreased by half of that modeled in the absence of competing sites:

$$M = m_{50,\rho} + \sum_i \frac{m_{50,\rho}}{K_{D,i} + m_{50,\rho} B} T + \frac{m_{50,\rho}}{K_{D,e} + m_{50,\rho}} \mathrm{IC}_{50,\rho} \ , \qquad [2.25]$$

where $m_{50,e}$ satisfies the relationship

$$\rho_e(m_{50,\rho}) = \frac{2\rho_e(m_0)}{\rho_e(m_0)+1} \ , \qquad [2.26]$$

from equation [1.12] describing the calculation of IC_{50} from the dual-reporter experiments. This also yields

$$m_{50,\rho} = \frac{K_{D,i} m_0}{m_0 + 2K_{D,i}} \ , \qquad [2.27]$$

demonstrating that the IC_{50} for repression calculated in the previous section reports on the IC_{50} for occupancy, without directly monitoring occupancy. Indeed, equation [2.18], which describes the level of repression within the steady-state model, can be rearranged and substituted with equation [2.17] yielding an equivalent form as the empirical definition of repression expressed in equation [1.5]:

$$\rho_i = \frac{1}{1 + \theta_i \left(B_i - 1 \right)} \ , \qquad [2.28]$$

demonstrating that R from equation [1.5] is proportional to θ, and so must have equivalent half-maximal competition values.

The DRT (represented by the dashed vertical lines in the left and middle panels of Figure 7A) was defined as the abundance of competing site at which the apparent rate of miRNA-mediated degradation of the target has decreased to 90% of its maximum value on a logarithmic scale:

$$M = m_{\mathrm{DRT}} + \sum_i \frac{m_{\mathrm{DRT}}}{K_{\mathrm{D},i} + m_{\mathrm{DRT}}} T_i + \frac{m_{\mathrm{DRT}}}{K_{\mathrm{D},e} + m_{\mathrm{DRT}}} \mathrm{DRT} \ , \qquad [2.29]$$

where

$$\rho_e(m_{DRT}) = \left(\rho_e(m_0)\right)^{\frac{9}{10}} \qquad [2.30]$$

For the mixed affinity model of miR-293 in ESCs, parameter values were as follows: B = 3.9, T'_{8nt} = 1.31 x 10^3 cpc, T'_{7nt} = 7.88 x 10^3, T'_{6nt} = 1.18 x 10^4, T'_{la} = 4.12 x 10^6, $K_{D,8nt}$ = 2.27 cpc, $K_{D,7nt}$ = 4.54 cpc, $K_{D,6nt}$ = 11.3 cpc, and $K_{D,la}$ = 6.80 x 10^2 cpc, with M = 8.22 x 10^2 cpc (light blue curve), 2.60 x 10^3 cpc (blue curve), or 8.22 x 10^3 (dark blue curve), and T'_e ranging from 10^2 to 10^5 cpc. For the occupancy model adapted from Bosson et al. (2014), parameter values were as follows: T'_{la} = 5.00 x 10^6 cpc and $K_{D,la}$ = 5.83 x 10^2 cpc, with M = 8.31 x 10^2 cpc (light blue curve), 2.63 x 10^3 cpc (blue curve), or 8.31 x 10^3 (dark blue curve), and T'_e ranging from 10^2 to 10^5 cpc. For the model adapted from Jens and Rajewsky (2015), parameter values were as follows: R_{vol} = 0.188, R_{TA} = 0.139, T'_{la} = 4.10 x 10^6 cpc, and $K_{D,la}$ = 2.31 x 10^3 cpc, with M = 8.22 x 10^2 cpc (light blue curve), 2.60 x 10^3 cpc (blue curve), or 8.22 x 10^3 (dark blue curve), and T'_e ranging from 10^2 to 10^5 cpc.

SUPPLEMENTAL REFERENCES

Ala, U., Karreth, F.A., Bosia, C., Pagnani, A., Taulli, R., Leopold, V., Tay, Y., Provero, P., Zecchina, R., and Pandolfi, P.P. (2013). Integrated transcriptional and competitive endogenous RNA networks are cross-regulated in permissive molecular environments. Proc Natl Acad Sci U S A *110*, 7154-7159.

Bosson, A.D., Zamudio, J.R., and Sharp, P.A. (2014). Endogenous miRNA and target concentrations determine susceptibility to potential ceRNA competition. Mol Cell *56*, 347-359.

Denzler, R., Agarwal, V., Stefano, J., Bartel, D.P., and Stoffel, M. (2014). Assessing the ceRNA hypothesis with quantitative measurements of miRNA and target abundance. Mol Cell *54*, 766-776.

Dobin, A., Davis, C.A., Schlesinger, F., Drenkow, J., Zaleski, C., Jha, S., Batut, P., Chaisson, M., and Gingeras, T.R. (2013). STAR: ultrafast universal RNA-seq aligner. Bioinformatics *29*, 15-21.

Hong, S., Pan, Q., and Lee, L.P. (2012). Single-cell level co-culture platform for intercellular communication. Integr Biol (Camb) *4*, 374-380.

Jens, M., and Rajewsky, N. (2015). Competition between target sites of regulators shapes post-transcriptional gene regulation. Nat Rev Genet *16*, 113-126.

Krutzfeldt, J., Rajewsky, N., Braich, R., Rajeev, K.G., Tuschl, T., Manoharan, M., and Stoffel, M. (2005). Silencing of microRNAs in vivo with 'antagomirs'. Nature *438*, 685-689.

Krutzfeldt, J., Rosch, N., Hausser, J., Manoharan, M., Zavolan, M., and Stoffel, M. (2012). MicroRNA-194 is a target of transcription factor 1 (Tcf1, HNF1alpha) in adult liver and controls expression of frizzled-6. Hepatology *55*, 98-107.

Mukherji, S., Ebert, M.S., Zheng, G.X., Tsang, J.S., Sharp, P.A., and van Oudenaarden, A. (2011). MicroRNAs can generate thresholds in target gene expression. Nat Genet *43*, 854-859.

Pall, G.S., and Hamilton, A.J. (2008). Improved northern blot method for enhanced detection of small RNA. Nat Protoc *3*, 1077-1084.

Salomon, W.E., Jolly, S.M., Moore, M.J., Zamore, P.D., and Serebrov, V. (2015). Single-Molecule Imaging Reveals that Argonaute Reshapes the Binding Properties of Its Nucleic Acid Guides. Cell *162*, 84-95.

Schmiedel, J.M., Klemm, S.L., Zheng, Y., Sahay, A., Bluthgen, N., Marks, D.S., and van Oudenaarden, A. (2015). Gene expression. MicroRNA control of protein expression noise. Science *348*, 128-132.

Schwanhausser, B., Busse, D., Li, N., Dittmar, G., Schuchhardt, J., Wolf, J., Chen, W., and Selbach, M. (2011). Global quantification of mammalian gene expression control. Nature *473*, 337-342.

Title, A.C., Denzler, R., and Stoffel, M. (2015). Uptake and Function Studies of Maternal Milk-derived MicroRNAs. J Biol Chem *290*, 23680-23691.

Trapnell, C., Hendrickson, D.G., Sauvageau, M., Goff, L., Rinn, J.L., and Pachter, L. (2013). Differential analysis of gene regulation at transcript resolution with RNA-seq. Nature Biotechnology *31*, 46-+.

Zhang, W., Sargis, R.M., Volden, P.A., Carmean, C.M., Sun, X.J., and Brady, M.J. (2012). PCB 126 and other dioxin-like PCBs specifically suppress hepatic PEPCK expression via the aryl hydrocarbon receptor. PLoS One *7*, e37103.